Westinghouse Non-Proprietary Class 3

WCAP-16038-NP
Revision 0

March 2003

Structural Integrity Evaluation of Reactor Vessel Upper Head Penetrations to Support Continued Operation: St. Lucie Unit 2

Westinghouse

WCAP-16038-NP
Revision 0

Structural Integrity Evaluation of Reactor Vessel Upper Head Penetrations to Support Continued Operation: St. Lucie Unit 2

S. Jirawongkraisorn
C. K. Ng

March 2003

Verifier: _____
R. Kabir
Structural Mechanics Technology

Approved: _____
S. A. Swamy
Structural Mechanics Technology

Westinghouse Electric Company LLC
P.O. Box 355
Pittsburgh, PA 15230-0355

TABLE OF CONTENTS

TABLE OF CONTENTS (Cont.)

LIST OF TABLES

LIST OF FIGURES

LIST OF FIGURES (Cont.)

LIST OF FIGURES (Cont.)

LIST OF FIGURES (Cont.)

LIST OF FIGURES (Cont.)

1 INTRODUCTION

In September of 1991, a leak was discovered in the Reactor Vessel Control Rod Drive Mechanism (CRDM) head penetration region of an operating plant. This has led to the question of whether such a leak could occur at the St. Lucie Unit 2 Control Element Drive Mechanism (CEDM), In-Core Instrumentation (ICI), or head vent nozzle penetrations. Note that the designation CRDM (Westinghouse and French designs) and CEDM (Combustion Engineering Design) are synonymous. The geometry of interest is shown in Figure 1-1. Throughout this report, the penetration rows have been identified by their angle of intersection with the head. The location of head penetrations for St. Lucie Unit 2 is shown in Figure 1-2 and the angles for each penetration are identified in Table 1-1.

The CEDM leak resulted from cracking in Alloy 600 base metal, which occurred in the outermost penetrations of a number of operating plants as discussed in Section 2. This outermost CEDM location, as well as a number of intermediate CEDM locations, the ICI nozzles, and the head vent were chosen for fracture mechanics analyses to support continued safe operation of St. Lucie Unit 2 if such cracking were to be found. The dimensions of the CEDM penetrations are all identical, with a 4.050 inch Outside Diameter (OD) and a wall thickness of 0.661 inch [11B]. The ICI penetrations have an OD of 5.563 inch and wall thickness of 0.469 inch [11A]; however, they all have a counterbore of 0.407 inch which extend to more than 12 inches from the bottom of the tube. For this reason, the counterbore thickness shall be used when evaluating all ICI nozzle flaws. The head vent OD is 1.050 inch and the wall thickness is 0.154 inch [11C]. All of these dimensions are summarized in Table 6-2.

The basis of the fracture analysis was a detailed three-dimensional elastic-plastic finite element analysis of several penetration locations, as described in detail in Section 5. The fracture analysis was carried out using crack growth rates recommended by the EPRI Materials Reliability Program (MRP). These rates are consistent with service experience. The results are presented in the form of flaw tolerance charts for both surface and through wall flaws. If indications are found, the charts will determine the allowable service life of safe operation. The service life calculated in the flaw tolerance charts are all in Effective Full Power Years (EFPY).

Note that there are several locations in this report where proprietary information has been bracketed and deleted. For each of the bracketed locations, reasons for proprietary classifications are given using a standardized system. The proprietary brackets are labeled with three different letters to provide this information. The explanation for each letter is given below:

a. The information reveals the distinguishing aspects of a process or component, structure, tool, method, etc., and the prevention of its use by Westinghouse's competitors, without license from Westinghouse, gives Westinghouse a competitive economic advantage.

b. The information, if used by a competitor, would reduce the competitor's expenditure of resources or improve the competitor's advantage in the design, manufacture, shipment, installation, assurance of quality, or licensing of a similar product.

c. The information reveals aspects of past, present, or future Westinghouse or customer funded development plans and programs of potential commercial value to Westinghouse.

Table 1-1 St. Lucie Unit 2 Head Penetration Nozzles with the Intersection Angles Identified

Nozzle No.	Type	Angle (Degrees)	Nozzle No.	Type	Angle (Degrees)	Nozzle No.	Type	Angle (Degrees)
1	CEDM	0.0	35	CEDM	25.2	69	CEDM	42.4
2	CEDM	7.8	36	CEDM	29.1	70	CEDM	42.4
3	CEDM	7.8	37	CEDM	29.1	71	CEDM	42.4
4	CEDM	11.0	38	CEDM	29.1	72	CEDM	42.4
5	CEDM	11.0	39	CEDM	29.1	73	CEDM	42.4
6	CEDM	11.0	40	CEDM	29.1	74	CEDM	42.4
7	CEDM	11.0	41	CEDM	29.1	75	CEDM	42.4
8	CEDM	15.6	42	CEDM	29.1	76	CEDM	42.4
9	CEDM	15.6	43	CEDM	29.1	77	CEDM	42.4
10	CEDM	15.6	44	CEDM	32.6	78	CEDM	42.4
11	CEDM	15.6	45	CEDM	32.6	79	CEDM	42.4
12	CEDM	17.6	46	CEDM	32.6	80	CEDM	43.4
13	CEDM	17.6	47	CEDM	32.6	81	CEDM	43.4
14	CEDM	17.6	48	CEDM	33.8	82	CEDM	43.4
15	CEDM	17.6	49	CEDM	33.8	83	CEDM	43.4
16	CEDM	17.6	50	CEDM	33.8	84	CEDM	43.4
17	CEDM	17.6	51	CEDM	33.8	85	CEDM	43.4
18	CEDM	17.6	52	CEDM	33.8	86	CEDM	43.4
19	CEDM	17.6	53	CEDM	33.8	87	CEDM	43.4
20	CEDM	22.4	54	CEDM	33.8	88	CEDM	49.7
21	CEDM	22.4	55	CEDM	33.8	89	CEDM	49.7
22	CEDM	22.4	56	CEDM	34.9	90	CEDM	49.7
23	CEDM	22.4	57	CEDM	34.9	91	CEDM	49.7
24	CEDM	23.9	58	CEDM	34.9	92	ICI	55.3
25	CEDM	23.9	59	CEDM	34.9	93	ICI	55.3
26	CEDM	23.9	60	CEDM	37.1	94	ICI	55.3
27	CEDM	23.9	61	CEDM	37.1	95	ICI	55.3
28	CEDM	25.2	62	CEDM	37.1	96	ICI	55.3
29	CEDM	25.2	63	CEDM	37.1	97	ICI	55.3
30	CEDM	25.2	64	CEDM	37.1	98	ICI	55.3
31	CEDM	25.2	65	CEDM	37.1	99	ICI	55.3
32	CEDM	25.2	66	CEDM	37.1	100	ICI	55.3
33	CEDM	25.2	67	CEDM	37.1	101	ICI	55.3
34	CEDM	25.2	68	CEDM	42.4			

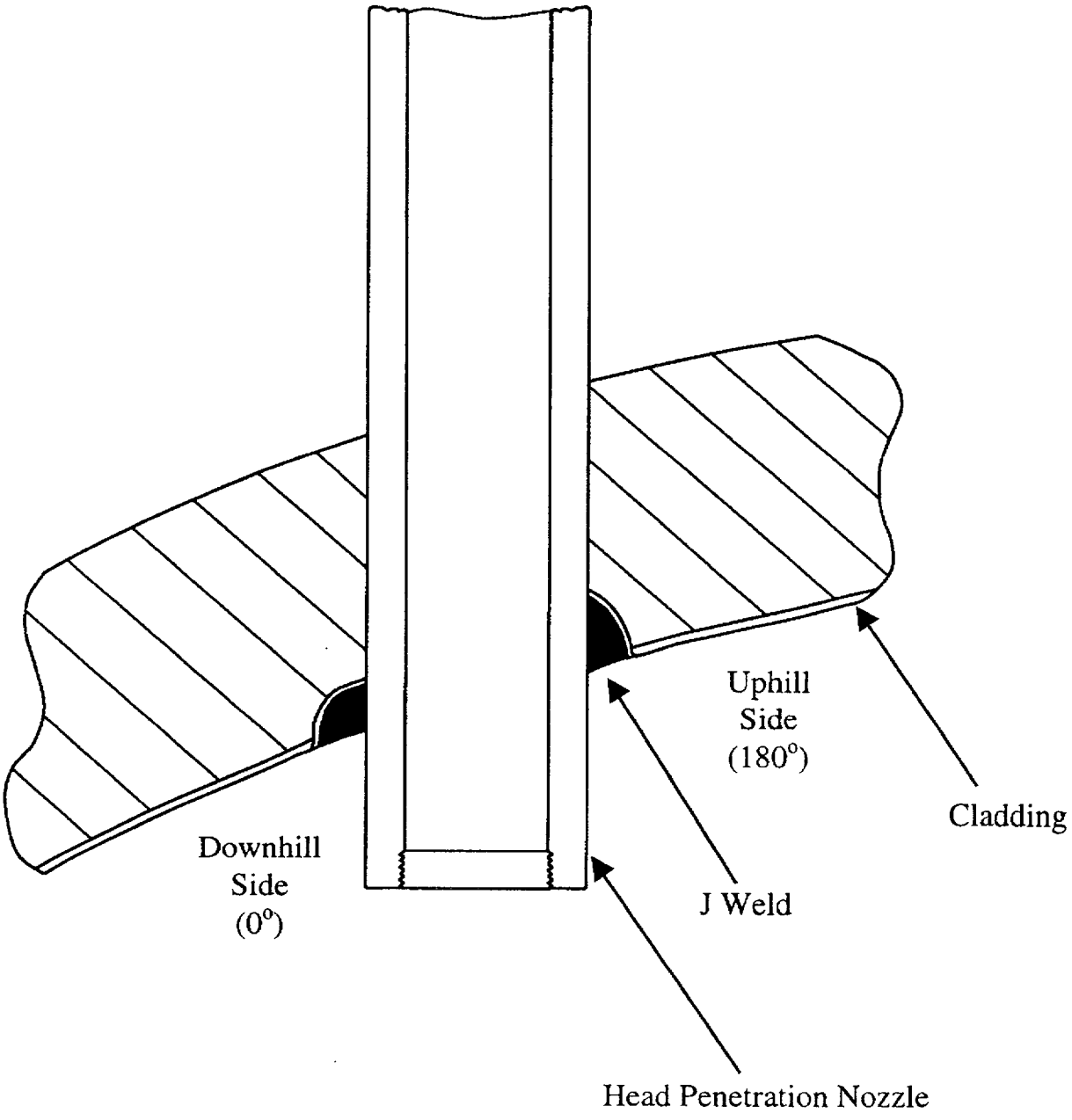

Figure 1-1 Reactor Vessel Control Element Drive Mechanism (CEDM) Penetration

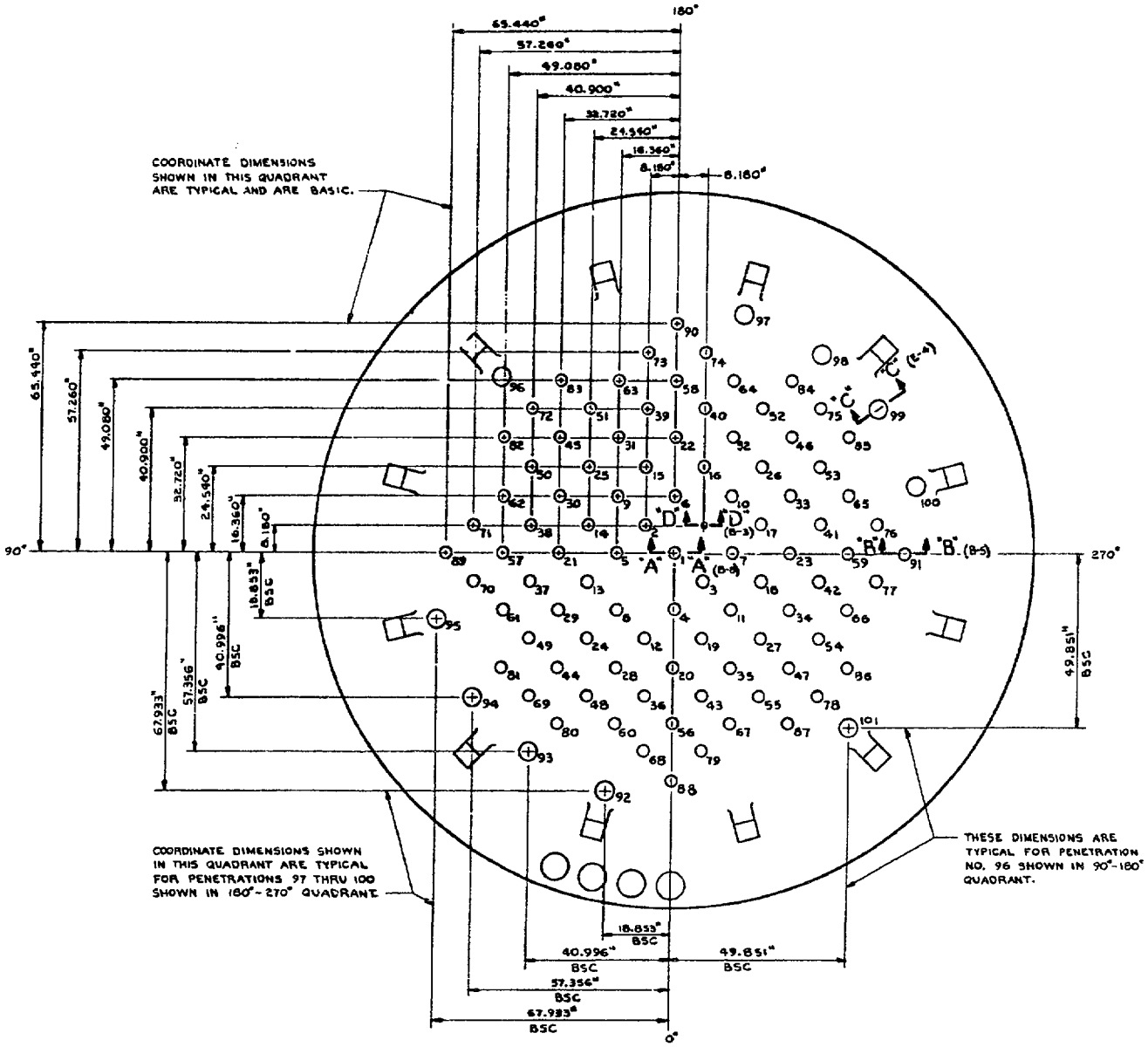

Figure 1-2 Location of Head Penetrations for St. Lucie Unit 2

2 HISTORY OF CRACKING IN HEAD PENETRATIONS

In September of 1991, leakage was reported from the reactor vessel CRDM head penetration region of a French plant, Bugey Unit 3. Bugey 3 is a 920 megawatt three-loop Pressurized Water Reactor (PWR) plant which had just completed its tenth fuel cycle. The leak occurred during a post ten year hydrotest conducted at a pressure of approximately 3000 psi (204 bar) and a temperature of 194°F (90°C). The leak was detected by metal microphones, which are located on the top and bottom heads. The leak rate was estimated to be approximately 0.7 liter/hour. The location of the leak was subsequently established on a peripheral penetration with an active control rod (H-14), as seen in Figure 2-1.

The control rod drive mechanism and thermal sleeve were removed from this location to allow further examination. A study of the head penetration revealed the presence of longitudinal cracks near the head penetration attachment weld. Penetrant and ultrasonic testing confirmed the cracks. The cracked penetration was fabricated from Alloy 600 bar stock (SB-166), and has an outside diameter of 4 inches (10.16 cm) and an inside diameter of 2.75 inches (7.0 cm).

As a result of this finding, all of the control rod drive mechanisms and thermal sleeves at Bugey 3 were removed for inspection of the head penetrations. Only two penetrations were found to have cracks, as shown in Figure 2-1.

An inspection of a sample of penetrations at three additional plants were planned and conducted during the winter of 1991-92. These plants were Bugey 4, Fessenheim 1, and Paluel 3. The three outermost rows of penetrations at each of these plants were examined, and further cracking was found in two of the three plants.

At Bugey 4, eight of the 64 penetrations examined were found to contain axial cracks, while only one of the 26 penetrations examined at Fessenheim 1 was cracked. The locations of all the cracked penetrations are shown in Figure 2-1. At the time, none of the 17 CRDM penetrations inspected at Paluel 3 showed indications of cracking, however subsequent inspections of the French plants have confirmed at least one crack in each operating plant.

Thus far, the cracking in reactor vessel heads not designed by Babcock and Wilcox (B&W) has been consistent in both its location and extent. All cracks discovered by nondestructive examination have been oriented axially, and have been located in the bottom portion of the penetration in the vicinity of the partial penetration attachment weld to the vessel head as shown schematically in Figure 1-1.

[

]^{a,c,e}

[

]a,c,e

Non-destructive examinations of the leaking CRDM nozzles showed that most of the cracks were axially oriented, originating on the outside surface of the nozzles below the J-groove weld and propagating primarily in the nozzle base material to an elevation above the top of the J-groove weld. Leakage could then pass through the annulus to the top of the head where it was detected by visual inspection. In some cases the cracks initiated in the weld metal or propagated into the weld metal, and in a few cases the cracks propagated through the nozzle wall thickness to the inside surface.

[

]a,c,e

[

]^{a,c,e}

The cracking has now been confirmed to be primary water stress corrosion cracking. Relatively high residual stresses are produced in the outermost CRDM penetrations due to the welding process. Other important factors which affect this process are temperature and time, with higher temperatures and longer times being more detrimental. The inspection findings for the plants examined through April 30th, 2002 are summarized in Table 2-1.

Table 2-1 Operational Information and Inspection Results for Units Examined (Results through April 30, 2002)

Country	Plant Type	Units Inspected	K Hours	Head Temp. (°F)	Total Penetrations	Penetrations Inspected	Penetrations With Indications
France	CPO	6	80-107	596-599	390	390	23
	CPY	28	42-97	552	1820	1820	126
	1300MW	20	32-51	558-597	1542	1542	95
Sweden	3 Loop	3	75-115	580-606	195	190	8
Switzerland	2 Loop	2	148-154	575	72	72	2
Japan	2 Loop	7	105-108	590-599	276	243	0
	3 Loop	7	99	610	455	398	0
	4 Loop	3	46	590	229	193	0
Belgium	2 Loop	2	115	588	98	98	0
	3 Loop	5	60-120	554-603	337	337	6
Spain	3 Loop	5	65-70	610	325	102	0
Brazil	2 Loop	1	25	NA	40	40	0
South Africa	3 Loop	1	NA	NA	65	65	6
Slovenia	2 Loop	1	NA	NA	49	49	0
South Korea	2 Loop	3	NA	NA	49	49	3
	3 Loop	2	NA	NA	130	130	2
US	2 Loop	2	170	590	98	98	0
	3 Loop	1	NA	NA	65	20	12
	4 Loop	18	NA	NA	1149	537	35
TOTALS		117	–	–	7384	6373	318

NA = Not Available.

Note: CPY and CPO are both 900 MW reactors.

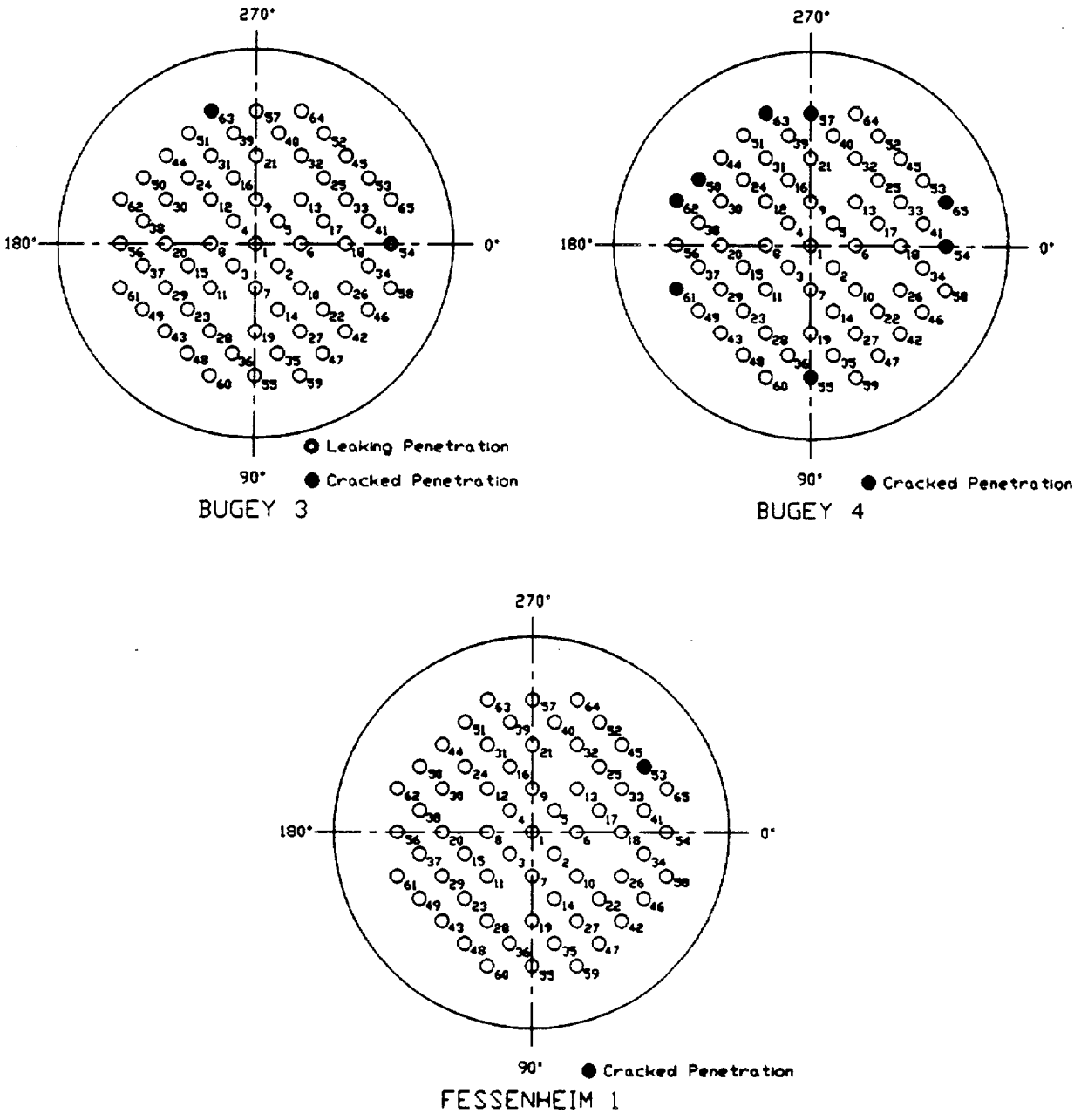

Figure 2-1 EDF Plant R/V Closure Head CEDM Penetrations – Penetrations with Cracking

3 OVERALL TECHNICAL APPROACH

The primary goal of this work is to provide technical justification for the continued safe operation of St. Lucie Unit 2 in the event that cracking is discovered during in-service inspections of the Alloy 600 reactor vessel upper head penetrations.

3.1 PENETRATION STRESS ANALYSIS

Three-dimensional elastic-plastic finite element stress analyses applicable to St. Lucie Unit 2 was performed to determine the stresses in the head penetration region [6A, 6B]. These analyses have considered the pressure loads associated with steady state operation, as well as the residual stresses that are produced by the fabrication process.

[

]^{a,c,e}

3.2 FLAW TOLERANCE APPROACH

A flaw tolerance approach has been developed to allow continued safe operation until an appropriate time for repair, or the end of plant life. The approach is based on the prediction of future growth of detected flaws, to ensure that such flaws would remain stable.

If an indication is discovered during in-service inspection, its size can be compared with the flaw size considered as allowable for continued service. This "allowable" flaw size is determined from the actual loading (including mechanical and residual loads) on the head penetration for St. Lucie Unit 2. Acceptance criteria are discussed in Section 6.5.

The time for the observed crack to reach the allowable crack size determines the length of time the plant can remain online before repair, if required. For the crack growth calculation, a best estimate is needed and no additional margins are necessary.

The results of the evaluation are presented in terms of simple flaw tolerance charts. The charts graphically show the time required to reach the allowable length or depth, which represents additional service life before repair. This result is a function of the loading on the particular head penetration as well as the circumferential location of the crack in the penetration nozzle.

Schematic drawings of the head penetration flaw tolerance charts are presented as Figures 3-1 and 3-2. These two types of charts can be used to provide estimates of the remaining service life before a leak would develop from an observed crack. For example, if a part-through flaw was discovered, the user would first refer to Figure 3-1, to determine the time (t_P) which would be remaining before the crack would penetrate the wall or reach the allowable depth (t_a) (e.g. a/t = 0.75). Once the crack penetrates the wall, the time (t_B) required to reach an allowable crack length would be determined from Figure 3-2. The total time remaining would then be the simple sum:

$$\text{Time remaining} = t_P + t_B$$

Another way to determine the allowable time of operation with a part-through flaw would be to use Figure 3-2 directly, in effect assuming the part-through flaw is a through-wall flaw. This approach would be more conservative than that above, and the time remaining would then be:

$$\text{Time remaining} = t_B$$

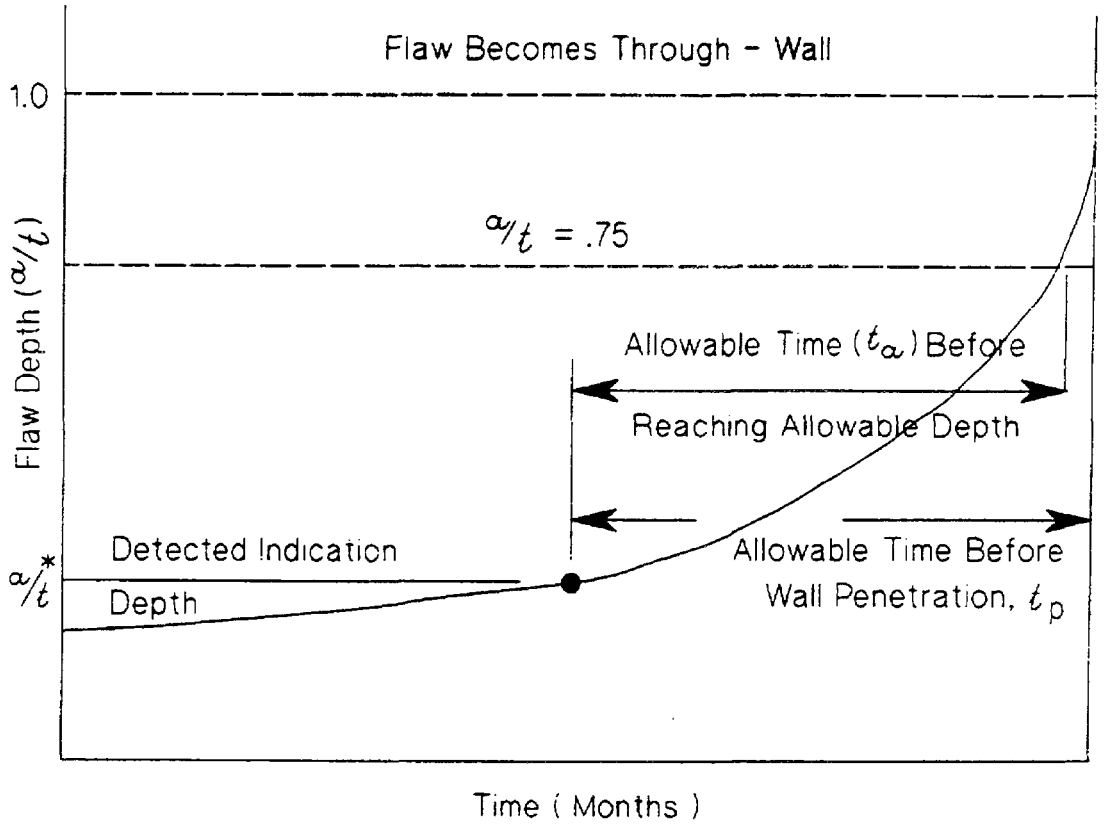

Figure 3-1 Schematic of a Head Penetration Flaw Growth Chart for Part-Through Flaws

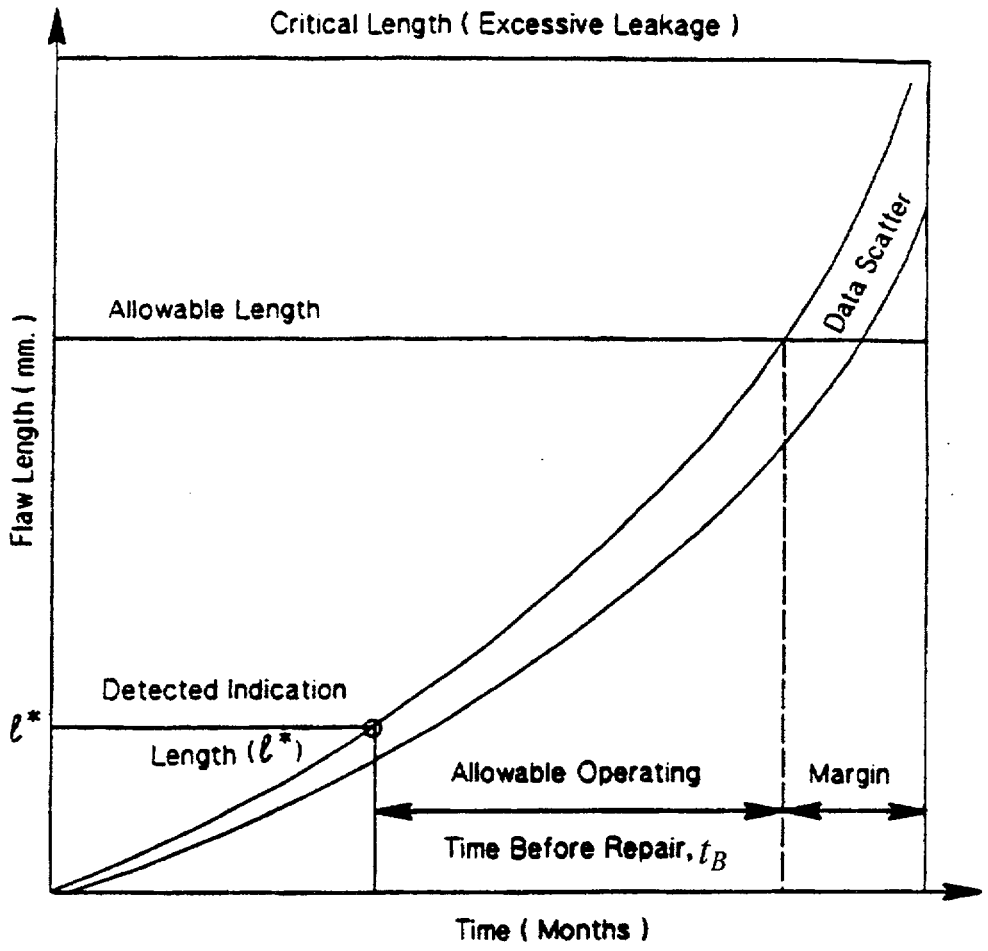

Figure 3-2 Schematic of a Head Penetration Flaw Tolerance Chart for Through-Wall Flaws

4 MATERIAL PROPERTIES, FABRICATION HISTORY AND CRACK GROWTH PREDICTION

4.1 MATERIALS AND FABRICATION

The head adapters for St. Lucie Unit 2 were produced by Standard Steel and Huntington Alloys in the USA. The carbon content and mechanical properties of the Alloy 600 material used to fabricate the St. Lucie Unit 2 vessel are provided in Table 4-1. The CEOG Program to Address Alloy 600 Cracking of CEDM Penetrations report [12] was used to obtain the chemistry and mechanical properties for the vessel head penetrations. The report indicates that the material for a number of CEDM nozzles was heat treated at 1625°F for 4 hours and air-cooled. Figures 4-1 and 4-2 illustrate the yield strengths and carbon content based on percent of heats for St. Lucie Unit 2 relative to a sample of the French head adapters that have experienced cracking. The general trend for the head adapter penetrations in St. Lucie Unit 2 is of a higher carbon content, higher mill annealing temperature, and lower yield strength relative to those on the French vessels. These factors should all have a beneficial effect on the material resistance to PWSCC in the head penetrations.

4.2 CRACK GROWTH PREDICTION

The cracks in the penetration region have been determined to result from primary water stress corrosion cracking in the Alloy 600 base metal and, in some cases, the Alloy 182 weld metal. There are a number of available measurements of static load crack growth rates in primary water environment, and in this section the available results will be compared and a representative growth rate established.

Direct measurements of Stress Corrosion Cracking (SCC) growth rates in Alloy 600 are relatively rare. Also, care should be used when interpreting the results because the materials may be excessively cold worked, or the loading applied may be near or exceeding the limit load of the penetration nozzle, meaning there will be an interaction between tearing and crack growth. In these cases the crack growth rates may not be representative of service conditions.

The effort to develop a reliable crack growth rate model for Alloy 600 began in the spring of 1992, when the Westinghouse Owners Group began to develop a safety case to support continued operation of plants. At the time, there was no available crack growth rate data for head penetration materials, and only a few publications existed on growth rates of Alloy 600 in any product form.

The best available publication at that time was that of Peter Scott of Framatome, who had developed a growth rate model for PWR steam generator materials [1]. His model was based on a study of results obtained by McIlree, Rebak and Smialowska [2] who had tested short steam generator tubes which had been flattened into thin compact specimens.

An equation was fitted to the data of reference [2] for the results obtained in water chemistries that fell within the standard specification for PWR primary water. Results for chemistries outside the specification were not used. The following equation was fitted to the data at 330°C (626°F):

$$\frac{da}{dt} = 2.8 \times 10^{-11} (K - 9)^{1.16} \text{ m/sec} \qquad (4\text{-}1)$$

where:

K is in MPa$\sqrt{m}$

The next step was to correct these results for the effects of cold work. Based on work by Cassagne and Gelpi [3], Scott concluded that dividing the above equation by a factor of 10 would be appropriate to account for the effects of cold work. The crack growth law for 330°C (626°F) then becomes:

$$\frac{da}{dt} = 2.8 \times 10^{-12} (K - 9)^{1.16} \text{ m/sec} \qquad (4\text{-}2)$$

Scott further corrected this law for the effects of temperature. This forms the basis for the PWR Materials Reliability Program (MRP) recommended crack growth rate (CGR) curve for the evaluation of SCC where a power-law dependence on stress intensity factor was assumed [4H]. The MRP recommended CGR curve was used in this report for determining the primary water stress corrosion crack growth rate and a brief discussion on this recommended curve is as follows:

[

]^{a,c,e}

[

]^{a,c,e}

There is a general agreement that crack growth in Alloy 600 materials in the primary water environment can be modeled using a power-law dependence on stress intensity factor with differences in temperature accounted for by an activation energy (Arrhenius) model for thermally controlled processes. Figure 4-3 shows the recommended CGR curve along with the laboratory data from Huntington materials used to develop the curve.

[

]^{a,c,e}

[

]^{a,c,e}

The applicability of the MRP recommended model to head penetrations was recently confirmed by two independent approaches. The first was a collection of all available data from Standard Steel and Huntington Alloys materials tested over the past ten years [4H]. The results are shown in Figure 4-3, along with the Scott model for the test temperature.

The MRP crack growth curve was structured to bound 75 percent of the 26 heats for which test results were available. Fits were done on the results for each heat, and the constant term was determined for each heat. This was done to eliminate the concern that the curve might be biased from a large number of results from a single heat. The 75th percentile was then determined from these results. The MRP expert panel on crack growth endorsed the resulting curve unanimously in a meeting on March 6th and 7th 2002. This approach is consistent with the Section XI flaw evaluation philosophy, which is to make a best estimate prediction of future growth of a flaw. Margins are incorporated in the allowable flaw sizes. The entire data set is shown in Figure 4-3, where the data have been adjusted to a single temperature of 325°C.

A second independent set of data were used to validate the model, and these data were obtained from the two inspections carried out on penetration no. 75 of D.C. Cook Unit 2, which was first found to be cracked in 1994 [4G]. The plant operated for one fuel cycle before the penetration was repaired in 1996 and the flaw was measured again before being repaired. These results were used to estimate the PWSCC growth rate for both the length of the flaw and its depth. These two points are also shown in Figure 4-4, and are consistent with the laboratory data for Huntington materials. In fact, Figure 4-4 demonstrates that the MRP model is nearly an upper bound for these materials. The D.C. Cook Unit 2 penetrations were made from Huntington materials.

Since St. Lucie Unit 2 operates at a temperature of 313°C (596°F) in the head region [9], and the crack growth rate is strongly affected by temperature, a temperature adjustment is necessary. This temperature correction was obtained from study of both laboratory and field data for stress corrosion crack growth rates for Alloy 600 in primary water environments. The available data showing the effect of temperature are summarized in Figure 4-5. Most of the results shown here are from steam generator tube materials, with several sets of data from operating plants, and results from two heats of materials tested in a laboratory [4A].

Study of the data shown in Figure 4-5 results in an activation energy of 31-33 Kcal/mole, which can then be used to adjust for the lower operating temperature. This value is slightly lower than the generally accepted activation energy of 44-50 Kcal/mole used to characterize the effect of temperature on crack initiation, but the trend of the actual data for many different sources is unmistakable.

[

].[a,c,e] Therefore the following crack growth rate model was used for the St. Lucie Unit 2 head penetration for crack growth in all the cases analyzed.

$$\frac{da}{dt} = 1.59 \times 10^{-12} (K - 9)^{1.16} \quad m/sec$$

where:

K = applied stress intensity factor, in $MPa\sqrt{m}$

This equation implies a threshold for cracking susceptibility, K_{ISCC} = 9 $MPa\sqrt{m}$. The crack growth rate is applicable to propagation in both axial and circumferential directions. (a,c,e)

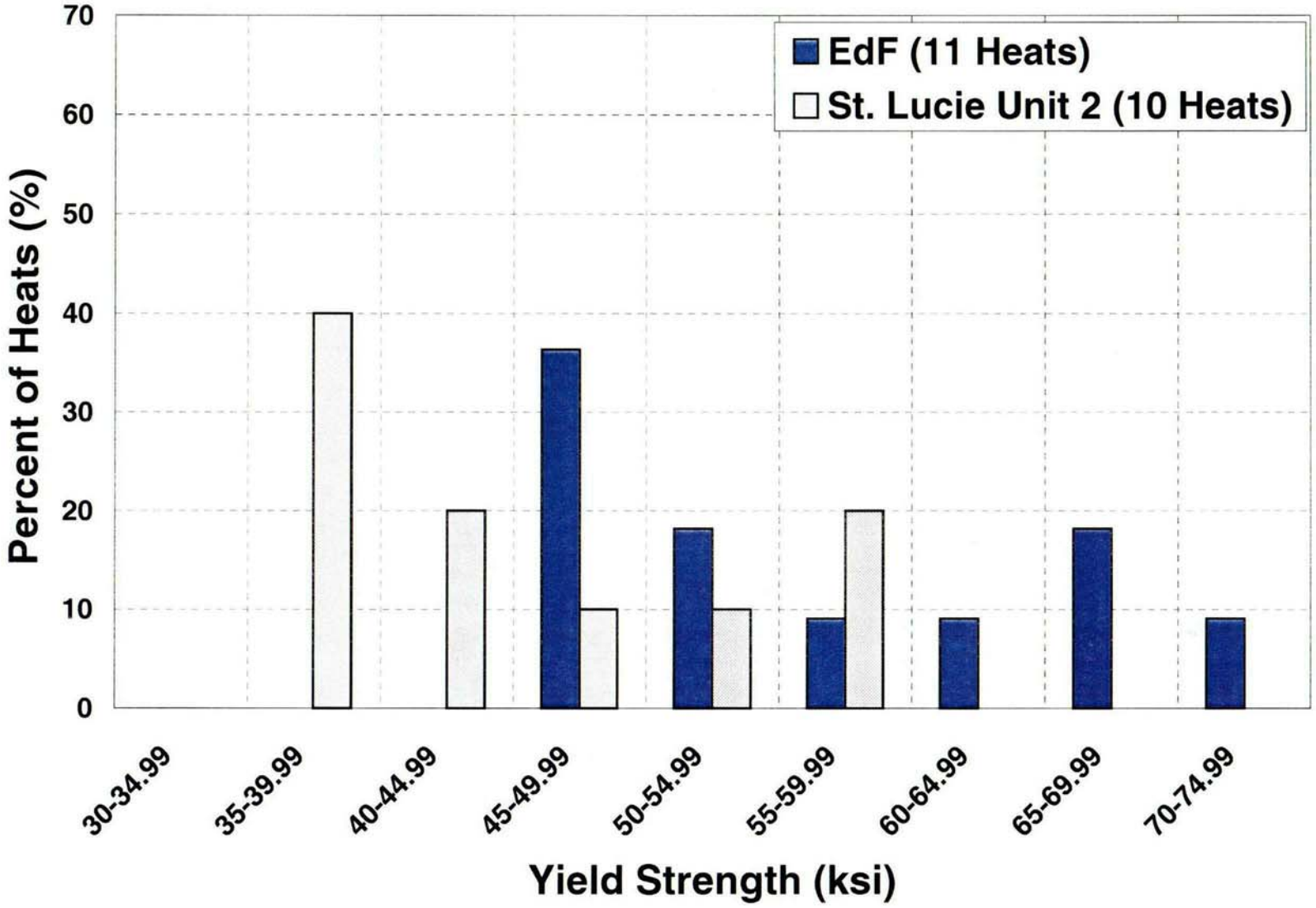

Figure 4-1 Yield Strength of the Various Heats of Alloy 600 Used in Fabricating the St. Lucie Unit 2 and French HeadPenetrations

C01

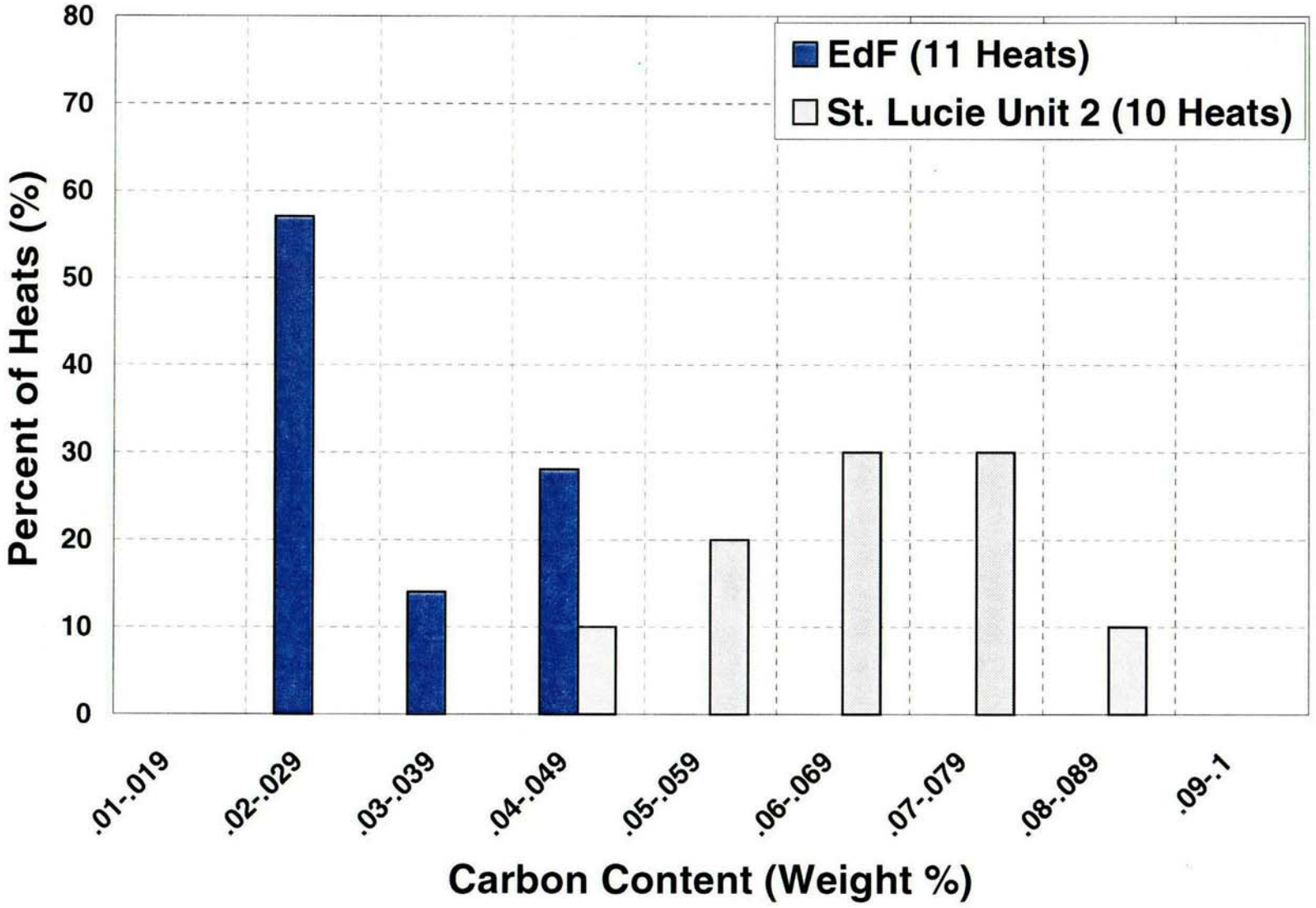

Figure 4-2 Carbon Content of the Various Heats of Alloy 600 Used in Fabricating the St. Lucie Unit 2 and French Head Penetration

C02

(a,c,e)

Figure 4-3 Screened Laboratory Data for Alloy 600 with the MRP Recommended Curve (Note that the Modified Scott Model is also Shown)

(a,c,e)

Figure 4-4 Model for PWSCC Growth Rates in Alloy 600 in Primary Water Environments (325°C), With Supporting Data from Standard Steel, Huntington, and Sandvik Materials

Note that the data have been normalized to a temperature of 325°C. The actual test temperatures are listed in parenthesis after the caption. For example, the Huntington data were obtained at temperature ranging from 315°C to 331°C.

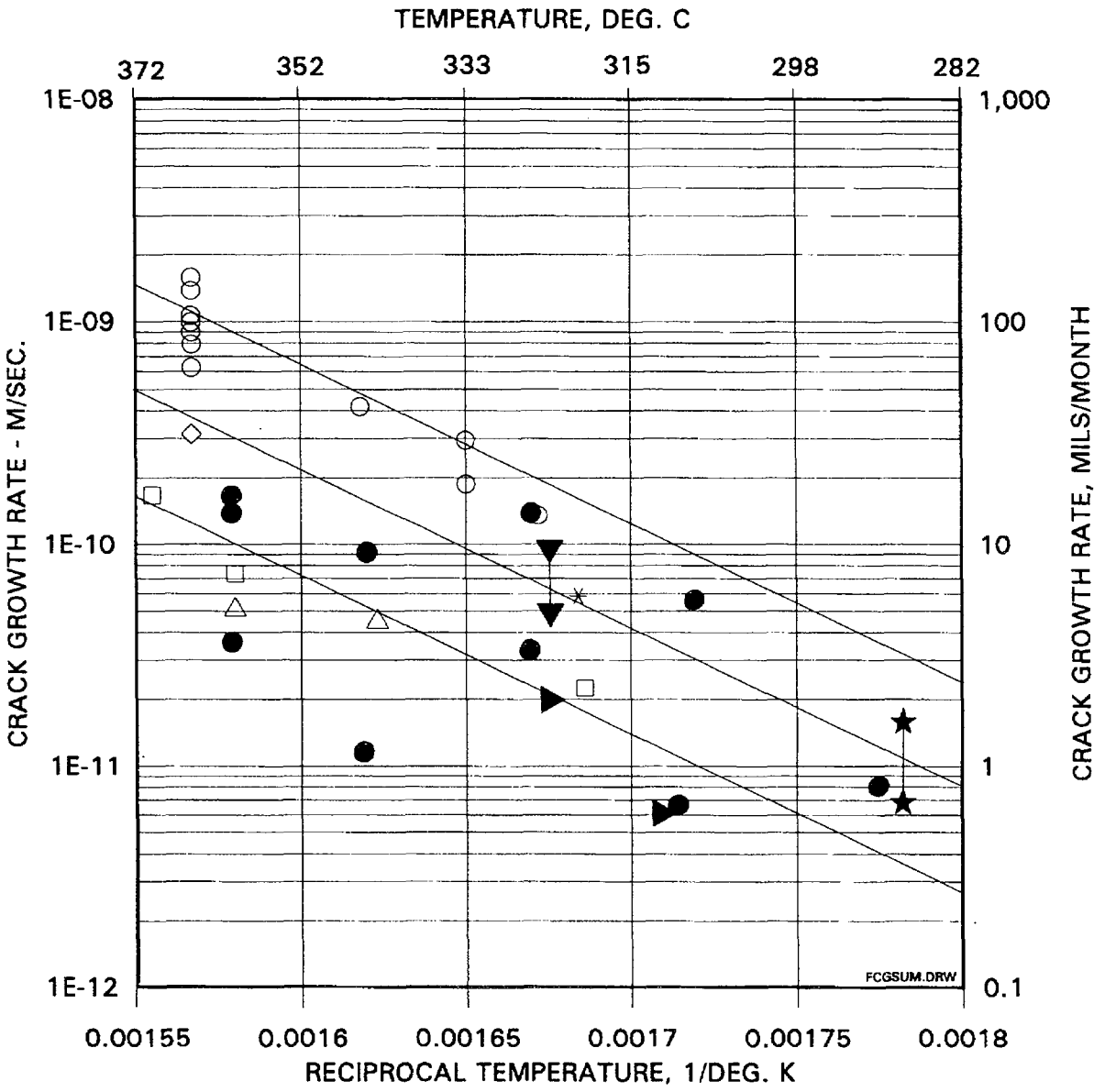

Note: All symbols are for steam generator materials, except the solid circles, which are head penetration laboratory data.

Figure 4-5 Summary of Temperature Effects on PWSCC Growth Rates for Alloy 600 in Primary Water

5 STRESS ANALYSIS

5.1 OBJECTIVES OF THE ANALYSIS

The objective of this analysis was to obtain accurate stresses in each of the CEDM and head vent penetrations as well as the immediate vicinity. To do so requires a three-dimensional finite element analysis which considers all the pertinent loading on the penetration [6]. An investigation of deformations at the lower end of the housing was also performed using the same model. Four CEDM locations were considered: the outermost row (49.7°), rows at 29.1°, 7.8°, and the center location (0°). These locations bound the CEDM penetration angles in the St. Lucie Unit 2 reactor vessel head. In addition, the ICI penetration (55.3°) and the head vent were analyzed.

The analyses were used to provide information for the flaw tolerance evaluation in Section 6. Also, the results of the stress analysis were compared to the findings from service experience to help assess the causes of the observed cracking.

5.2 MODEL

A three-dimensional finite element model comprised of isoparametric brick and wedge elements with mid-side nodes on each face was used to obtain the stresses and deflections. Views of CEDM and head vent models are shown in Figures 5-1 and 5-2 respectively. Taking advantage of the symmetry of the vessel head, only half of the CEDM penetrations were modeled. Similarly, only half of the center penetration was modeled.

In the models, the lower portion of the Control Element Drive Mechanism (CEDM) penetration nozzle, In-Core Instrumentation (ICI) nozzle, the head vent, the adjacent section of the vessel closure head, and the joining weld were modeled. The vessel to penetration nozzle weld was simulated with two layers of elements. The penetration nozzle, weld metal, and cladding were modeled as Alloy 600 and the vessel head shell as carbon steel.

The only loads used in the analysis are the steady state operating loads. External loads, such as seismic loads, have been studied and have no impact since the penetration nozzles are captured by the full thickness of the reactor vessel head (about 7 and 1/2 inches of steel [11D]) into which the penetrations are shrunk fit during construction. The area of interest is in the penetration near the attachment weld, which is unaffected by these external loads.

5.3 STRESS ANALYSIS RESULTS – OUTERMOST CEDM PENETRATION (49.7°)

Figure 5-4 presents the hoop and axial stresses for the steady state condition for the outermost CEDM penetration.

[

]^{a,c,e}

[

]^{a,c,e}

5.4 STRESS ANALYSIS RESULTS – INTERMEDIATE CEDM AND ICI PENETRATIONS

[

]^{a,c,e}

5.5 STRESS ANALYSIS RESULTS – CENTER CEDM PENETRATION

[

]^{a,c,e}

5.6 STRESS ANALYSIS RESULTS – HEAD VENT

[

]^{a,c,e}

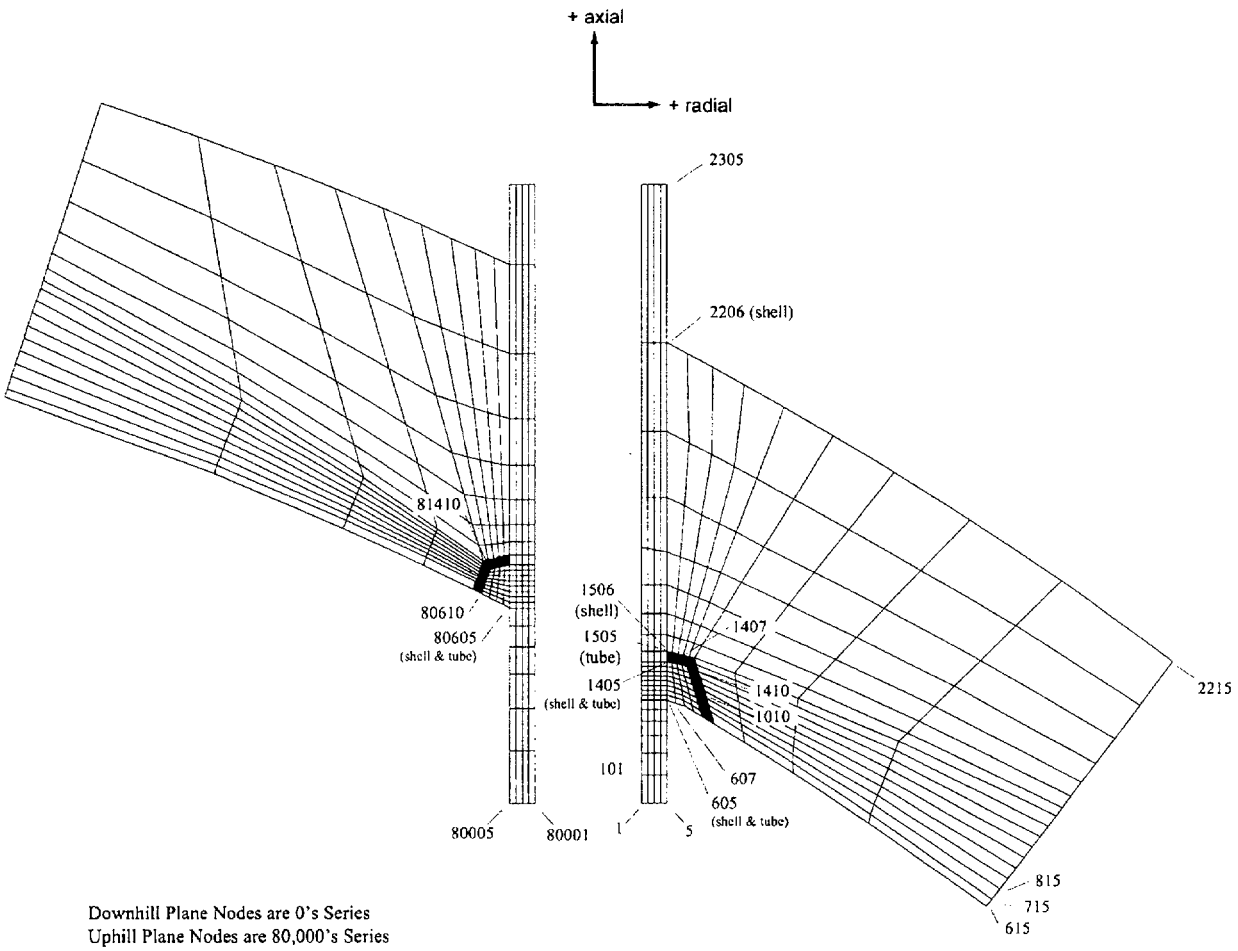

Downhill Plane Nodes are 0's Series
Uphill Plane Nodes are 80,000's Series

Tube Node Series: 1's at Nozzle ID, 5's at Nozzle OD
Shell Node Series: 5's at Shell ID (merged w/tube OD) in weld region
6's at Shell ID above weld region
15's at edge of shell section

Node Numbers Increase by 100 up the length of the tube and shell
Node Numbers Increase by 1 along the tube and shell radius

Figure 5-1 Finite Element Model of CEDM Penetration (29.1 Degrees)

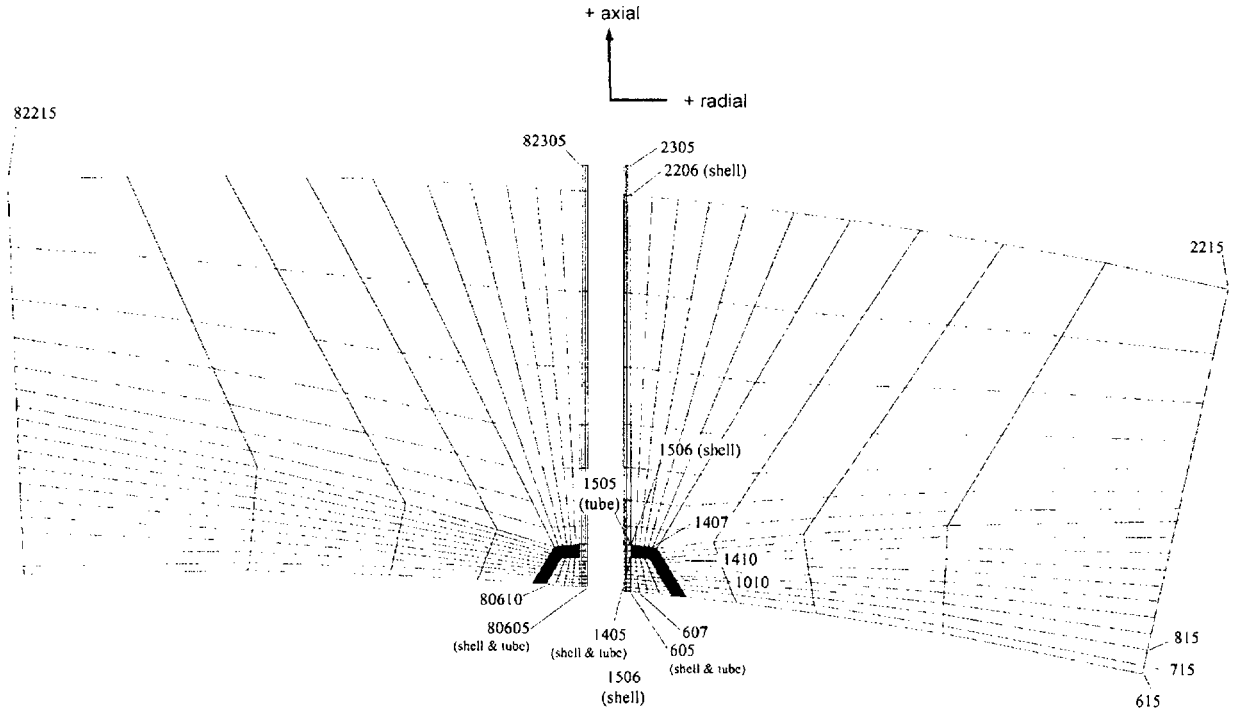

Downhill Plane Nodes are 0's Series
Uphill Plane Nodes are 80,000's Series

Tube Node Series: 1's at Nozzle ID, 5's at Nozzle OD
Shell Node Series: 5's at Shell ID (merged w/tube OD) in weld region
6's at Shell ID above weld region
15's at edge of shell section

Node Numbers Increase by 100 up the length of the tube and shell
Node Numbers Increase by 1 along the tube and shell radius

Figure 5-2 Vent Pipe Finite Element Model

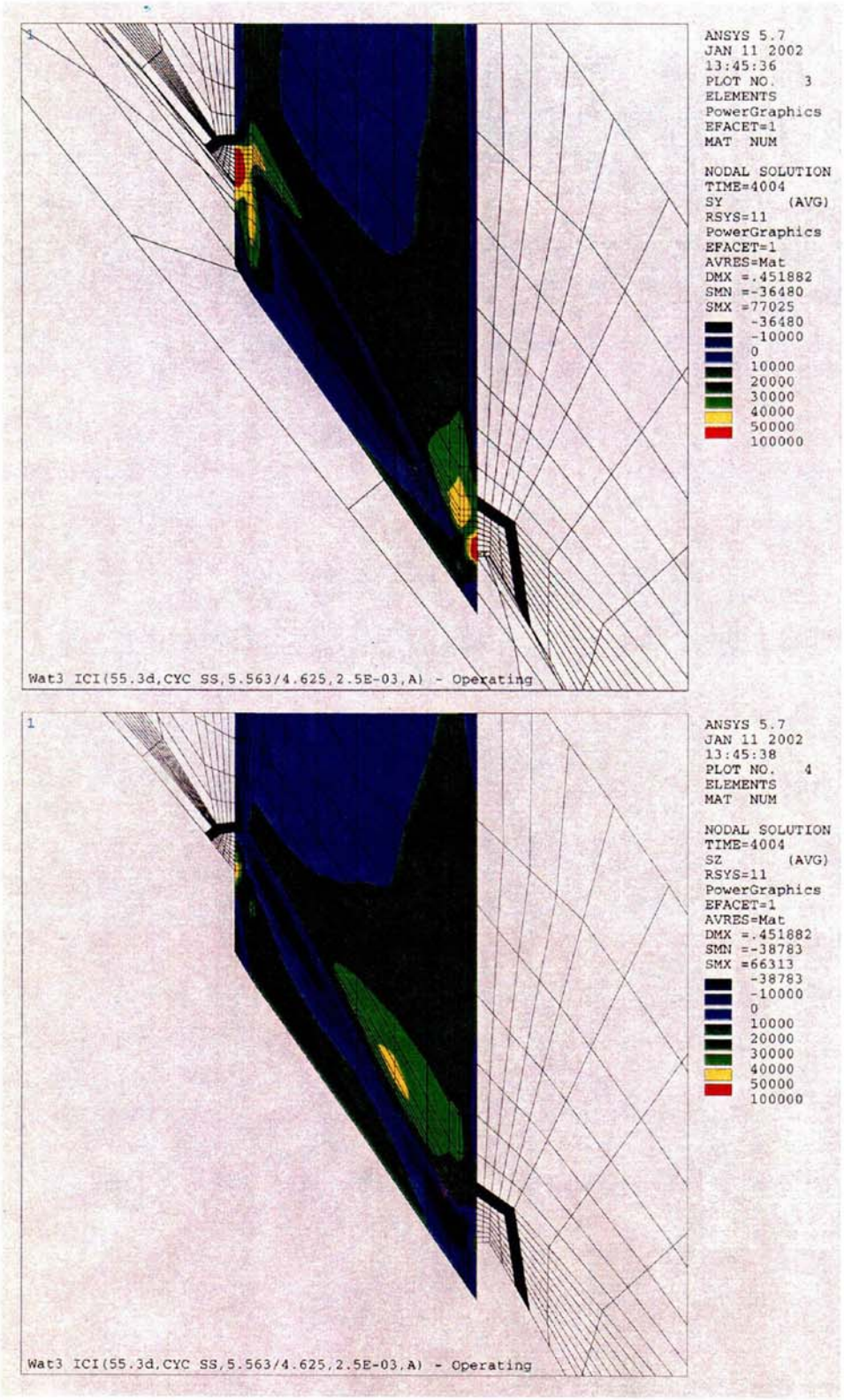

Figure 5-3 Stress Distribution at Steady State Conditions: ICI Penetration Nozzle (55.3 Degrees) (Hoop Stress is the Top Figure, Axial Stress is the Bottom Figure)

C03

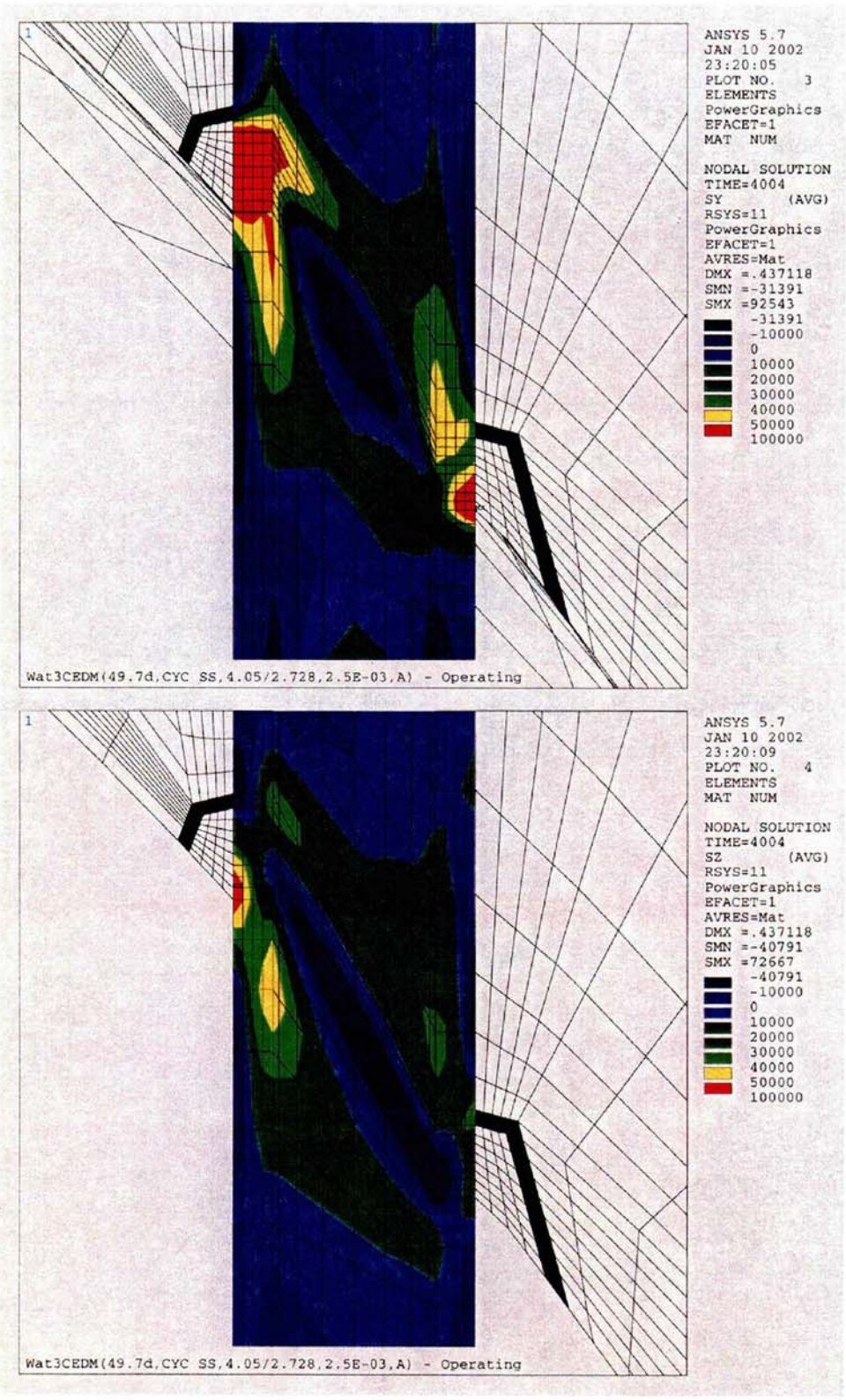

Figure 5-4 Stress Distribution at Steady State Conditions: Outermost CEDM Penetration Nozzle (49.7 Degrees) (Hoop Stress is the Top Figure; Axial Stress is the Bottom Figure)

C04

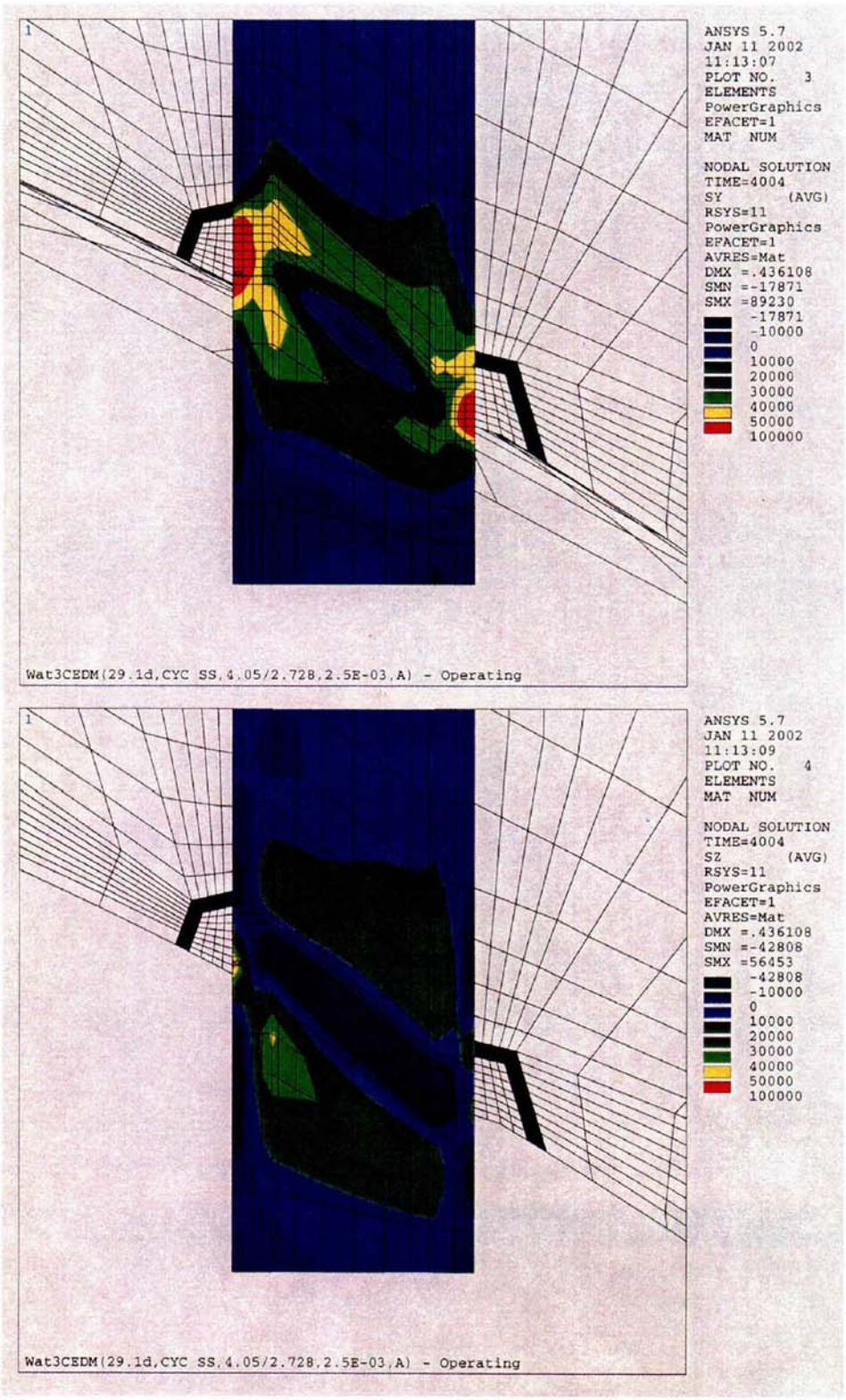

Figure 5-5 Stress Distribution at Steady State Conditions for the 29.1 Degrees CEDM Penetration (Hoop Stress is the Top Figure; Axial Stress is the Bottom Figure)

C05

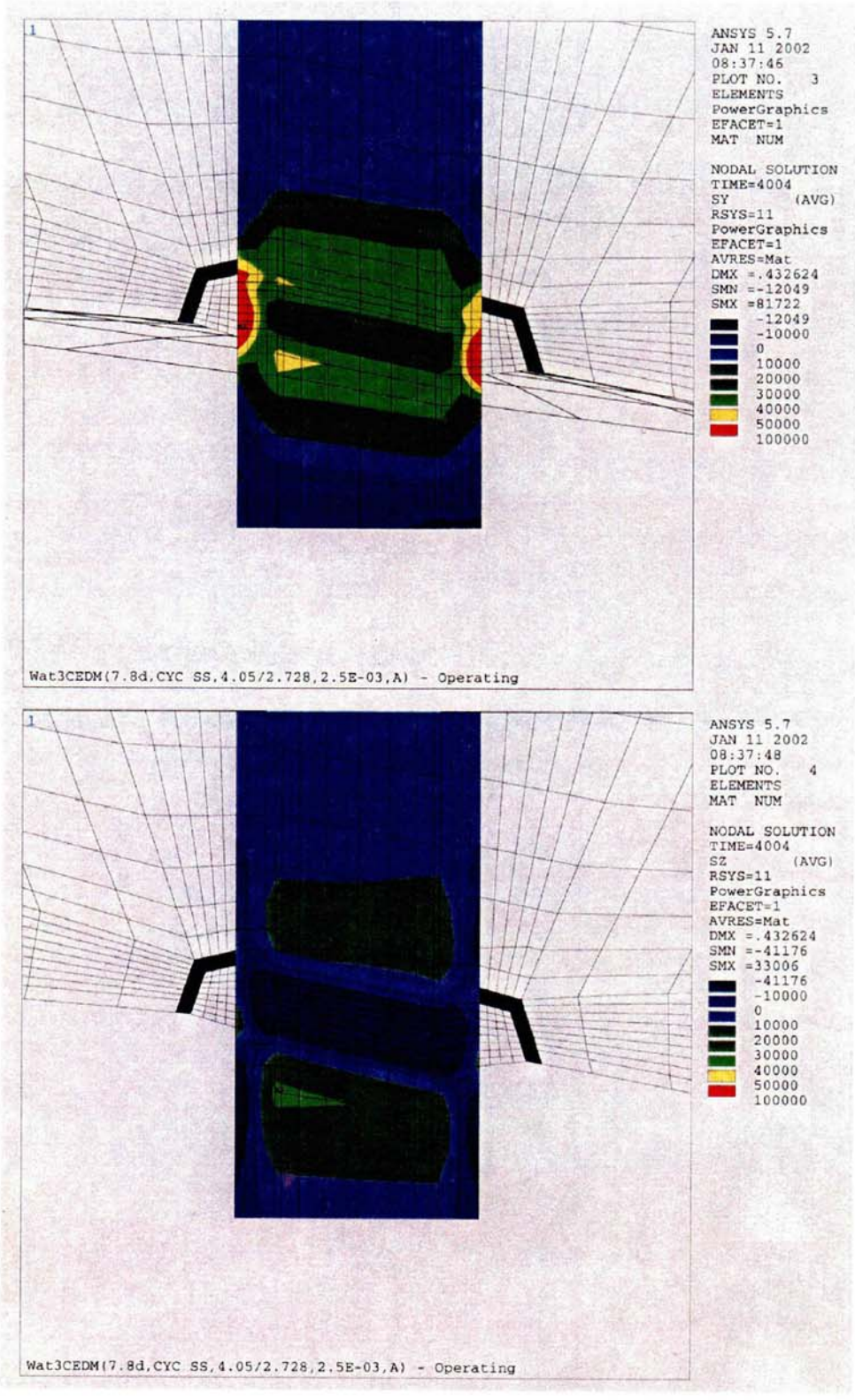

Figure 5-6 Stress Distribution at Steady State Conditions for the 7.8 Degrees CEDM Penetration (Hoop Stress is the Top Figure; Axial Stress is the Bottom Figure)

C06

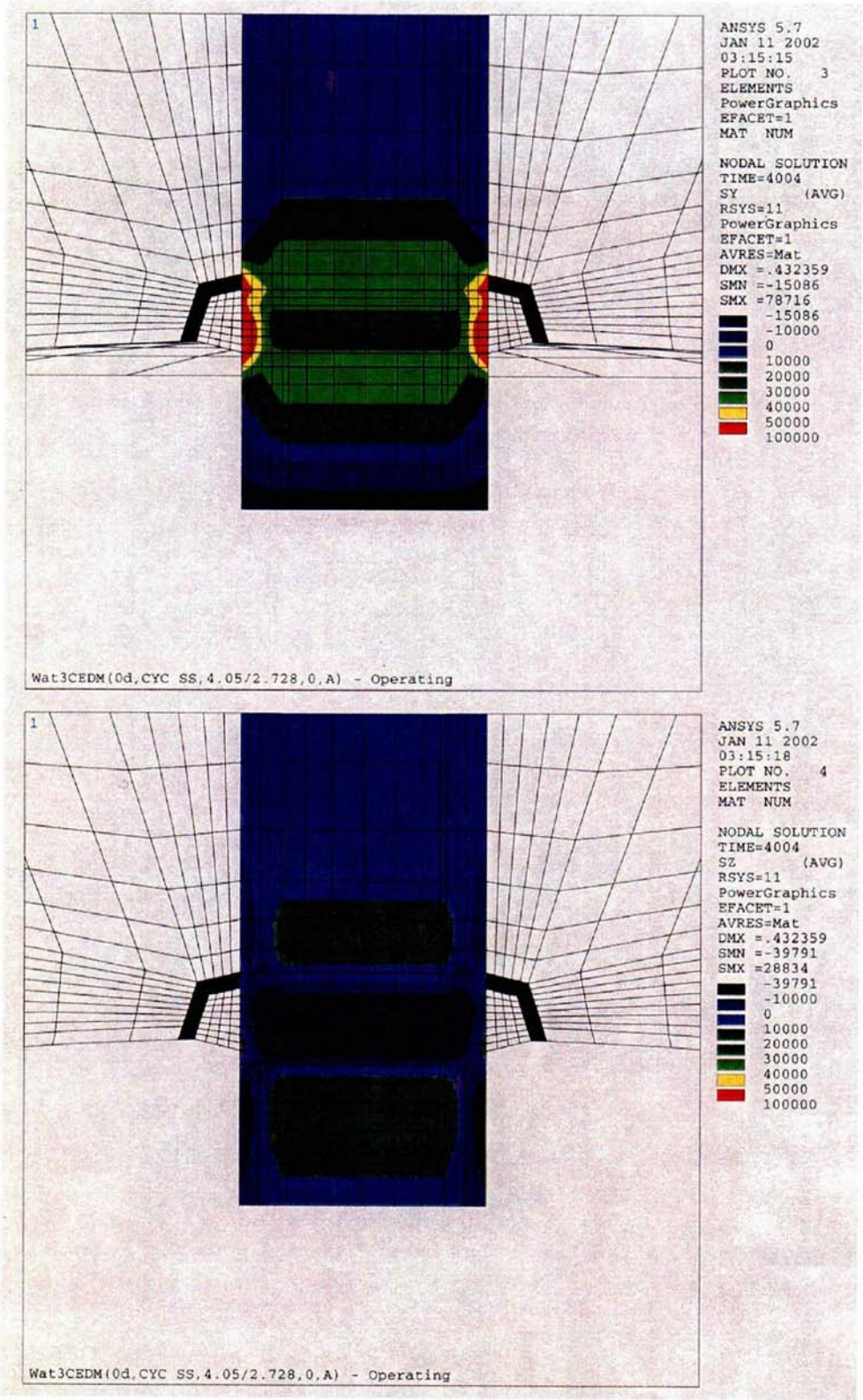

Figure 5-7 Stress Distribution at Steady State Conditions for the Center CEDM Penetration (Hoop Stress is the Top Figure; Axial Stress is the Bottom Figure)

C07

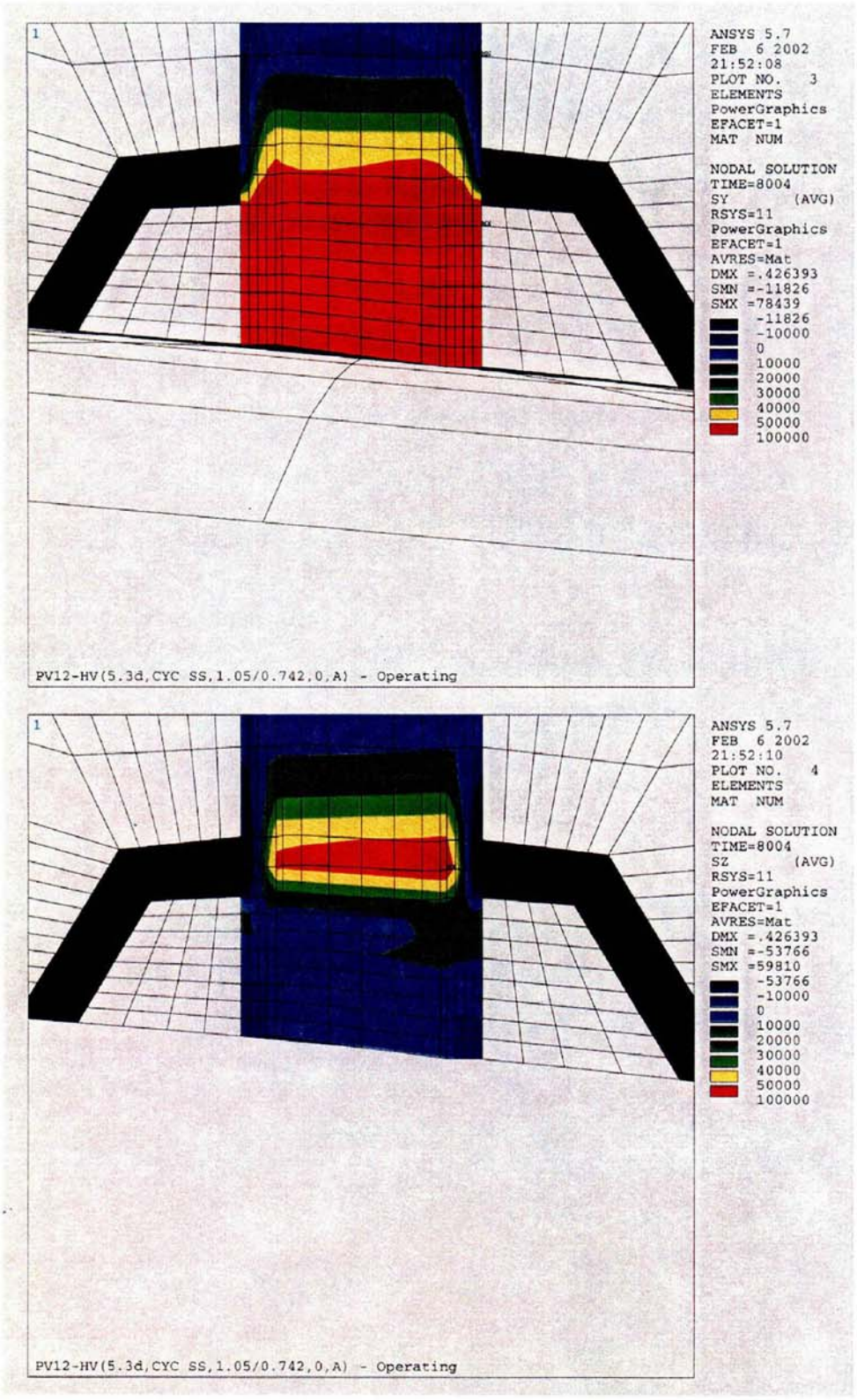

Figure 5-8 Stress Contours in the Head Vent Nozzle as a Result of Residual Stresses and Operating Pressure (Hoop Stress is the Top Figure; Axial Stress is the Bottom Figure)

C08

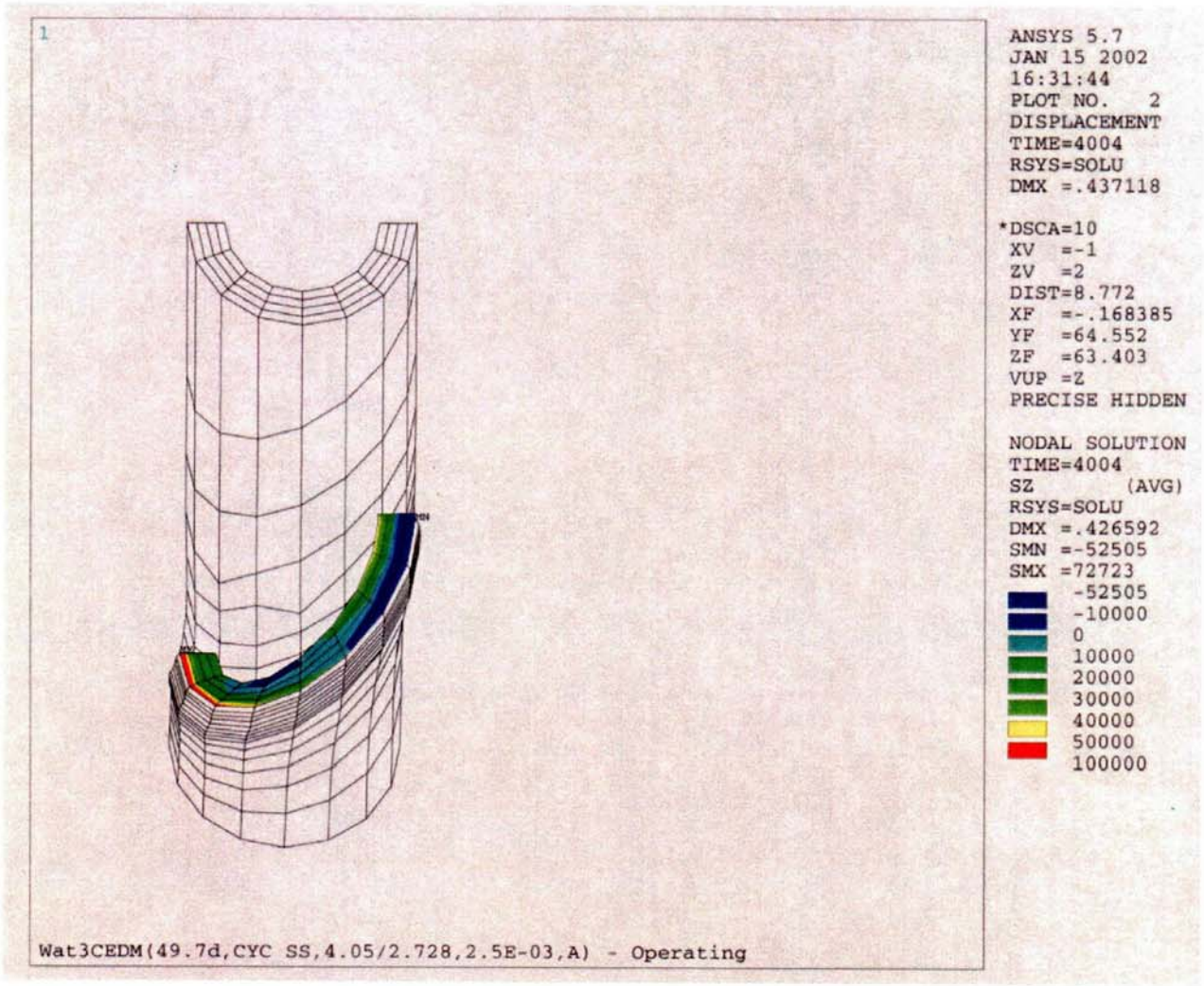

Figure 5-9 **Axial Stress Distribution at Steady State Conditions for the Outermost CEDM Penetration (49.7 Degrees), Along a Plane Oriented Parallel to, and Just Above, the Attachment Weld**

6 FLAW TOLERANCE CHARTS

6.1 INTRODUCTION

The flaw tolerance charts were developed using the stress analysis of each of the penetration locations as discussed in Section 5. The crack growth law developed for St. Lucie Unit 2 in Section 4.2 was used for each case, and several flaw tolerance charts were developed for each penetration location. The first series of charts characterizes the growth of a part through flaw, and the second series of charts characterizes the growth of a through-wall flaw in the length direction. The allowable safe operating life of the penetration nozzle may then be directly determined, using the combined results of the two charts. All times resulting from these calculations are effective full power years, since crack growth will only occur at operating temperatures.

6.2 OVERALL APPROACH

The results of the three-dimensional stress analysis of the penetration locations were used directly in the flaw tolerance evaluation.

The crack growth evaluation for the part-through flaws was based on the worst stress distribution through the penetration wall at the location of interest of the penetration. The highest stressed location was found to be in the immediate vicinity of the weld for both the center and outermost penetrations.

The stress profile was represented by a cubic polynomial:

$$\sigma(x) = A_0 + A_1 x + A_2 x^2 + A_3 x^3 \qquad (6\text{-}1)$$

where:

x = the coordinate distance into the nozzle wall
σ = stress perpendicular to the plane of the crack
A_I = coefficients of the cubic polynomial fit

For the surface flaw with length six times its depth, the stress intensity factor expression of Raju and Newman [5A] was used. The stress intensity factor $K_I(\Phi)$ can be calculated anywhere along the crack front. The point of maximum crack depth is represented by $\Phi = 0$, and this location was also found to be the point of maximum K_I for the cases considered here. The following expression is used for calculating $K_I(\Phi)$, where Φ is the angular location around the crack. The units of $K_I(\Phi)$ are $\text{ksi}\sqrt{\text{in}}$.

$$K_I(\Phi) = \left[\frac{\pi a}{Q}\right]^{0.5} \sum_{j=0}^{3} G_j\left(a/c,\ a/t,\ t/R,\ \Phi\right) A_j a^j \qquad (6\text{-}2)$$

The boundary correction factors $G_0(\Phi)$, $G_1(\Phi)$, $G_2(\Phi)$ and $G_3(\Phi)$ are obtained by the procedure outlined in reference [5A]. The dimension "a" is the crack depth, and "c" is the semi crack

length, while "t" is the wall thickness. "R" is the inside radius of the tube, and "Q" is the shape factor.

[

]^{a,c,e}

6.3 AXIAL FLAW PROPAGATION

CEDM and ICI Surface Flaws

The results of the calculated growth through the wall thickness of the CEDM penetration nozzles for surface flaws are shown in Figures 6-2 through 6-8 for inside surface flaws. For outside surface flaws the results are shown in Figures 6-9 and 6-10. Based on the discussion in MRP-55 report [4H], the use of stress intensity factors less than 15 MPa$\sqrt{m}$ involves assumption not currently substantiated by actual CGR data for neither CEDM nor ICI nozzle materials. Therefore, these crack growth curves begin at a flaw depth that results in a stress intensity factor of 15 MPa$\sqrt{m}$, which exceeds the threshold value of 9 MPa$\sqrt{m}$. This may result in curves with

different initial flaw sizes, as seen for example in Figure 6-3. Note that results are only provided for the uphill and downhill sides of each penetration nozzle; the stresses for the regions 90 degrees from these locations are compressive. If flaws are found in such a location, the results for either the uphill or downhill location, whichever is closer, can be used.

Each of these figures allows the future allowable service time to be estimated graphically, as discussed in Section 3. Results are shown for each of the penetration nozzles analyzed in each of these figures. The stresses are much higher near the attachment weld than at 0.5 inch below or above it, so separate figures have been provided for these three regions. For more than 0.5 inch below the weld, the crack growth will eventually come to rest since the stresses are compressive as shown for CEDM nozzles in Appendix E. Also, the stresses are different on the downhill side of the penetration as opposed to the uphill side, so these two cross sections have also been treated separately.

A set of guidelines for evaluating an indication found during inspection has been provided in Appendix B. Example problems following the previously mentioned guidelines are provided in Appendix C for a range of possible flaw types. In addition, worksheets for determining service life are given in Appendix D.

CEDM and ICI Through-Wall Flaws

The projected crack growth of a through-wall flaw in the CEDM and ICI penetration nozzles are the primary concern in evaluating the structural integrity of head penetrations. In some cases, the through-wall flaw may be located sufficiently below the attachment weld that additional time may be required for the flaw to grow to the attachment weld. To provide a means to evaluate the duration of this additional time, a series of flaw tolerance charts for through-wall flaws were prepared.

Charts were prepared for each of the penetrations evaluated, for both the uphill and downhill locations, as shown in Figures 6-12 through 6-20. In each figure, the through-wall crack length is measured from the bottom of the nozzle. Note that in all the cases, the crack slows down significantly as it grows above the weld, due to the decreasing magnitude of the stress field. This provides further assurance that axial flaws will not extend to a critical length which exceeds 15 inches, regardless of the duration of crack growth.

Head Vent

The only flaw tolerance chart that is necessary for the head vent region is for flaws at and above the weld, since there is no portion of the head vent which projects below the weld. Figure 6-8 provides the projected growth of a part through flaw in the head vent just above the attachment weld. The growth through the wall is relatively rapid, because the thickness of the head vent is small.

6.4 CIRCUMFERENTIAL FLAW PROPAGATION

Since circumferentially oriented flaws have been found at five plants (Bugey 3, Oconee 2, Crystal River 3, Davis Besse, and Oconee 3), it is important to consider the possibility of crack extension

in the circumferential direction. The first case was discovered as part of the destructive examination of the tube with the most extensive circumferential cracking at Bugey 3. The crack was found to have extended to a depth of 2.25 mm in a wall thickness of 16 mm. The flaw was found at the outside surface of the penetration (number 54) at the downhill side location, just above the weld.

The circumferential flaws in Oconee Unit 3 were discovered during the process of repairing a number of axial flaws, whereas the circumferential flaw in Oconee Unit 2 and Crystal River Unit 3 were discovered by UT. Experience gained from these findings has enabled the development of UT procedures capable of detecting circumferential flaws reliably.

To investigate this issue completely, a series of crack growth calculations were carried out for a postulated surface circumferential flaw located just above the head penetration weld, in a plane parallel to the weld itself. This is the only flaw plane that could result in a complete separation of the penetration nozzle, since all others would result in propagation below the weld, and therefore there is no chance of complete separation because the remaining weld would hold the penetration nozzle in place.

[

]^{a,c,e}

[

]^{a,c,e} The results of this calculation are shown in Figure 6-21. From Figure 6-21, it can be seen that the time required for propagation of a circumferential flaw to a point where the integrity of the CEDM penetration nozzle would be affected (330-350 degrees [10]) would be about 25 years. From the same figure, the required time for propagation of a circumferential flaw to a point where the integrity of the ICI penetration nozzles would be affected is about 37 years. Due to the conservatism in the calculations (the time period for a surface flaw to become a through-wall flaw was conservatively ignored) the service life is likely to be even longer. In addition, due to uncertainties in the exact composition of the chemical environment in contact with the nozzle OD, a multiplicative factor of 2.0 is used in the CGR for all circumferential surface flaws on the OD of the head penetration nozzles located above the elevation of the J-groove weld.

6.5 FLAW ACCEPTANCE CRITERIA

Now that the projected crack growth curves have been developed, the question remains as to what flaw size would be acceptable for further service.

Acceptance criteria have been developed for indications found during inspection of reactor vessel upper head penetration as part of an industry program coordinated by NEI (formerly NUMARC). Such criteria are normally found in Section XI of the ASME Code, but Section XI does not require in-service inspection of these regions and therefore acceptance criteria are not available. In developing the enclosed acceptance criteria, the approach used was very similar to that used by Section XI, in that an industry consensus was reached using input from both operating utility technical staff and each of the three PWR vendors. The criteria developed are applicable to all PWR plant designs.

Since the discovery of the leaks at Oconee and ANO-1, the acceptance criteria have been revised slightly to cover flaws on the outside diameter of the penetration below the attachment weld, and flaws in the attachment weld. These revised criteria are now in draft form, but they are expected to be acceptable to the NRC, and will be used in these evaluations. The draft portions of the acceptance criteria will be noted below.

The criteria presented herein are limits on flaw sizes, which are acceptable. The criteria are to be applied to inspection results. It should be noted that determination of the future service during which the criteria are satisfied is plant-specific and dependent on flaw geometry and loading conditions.

It has been previously demonstrated by each of the owners groups that the penetration nozzles are very tolerant of flaws and there is only a small likelihood of flaw extensions to larger sizes. Therefore, it was concluded that complete fracture of the penetration nozzle is highly unlikely. The approach used here is more conservative than that used in Section XI applications where the acceptable flaw size is calculated by placing a margin on the critical flaw size. For the current application, the critical flaw size would be far too large to allow a practical application of the approach used in Section XI applications, so protection against leakage is the priority.

The acceptance criteria presented herein apply to all the flaw types regardless of orientation and shape. Similar to the approach used in Section XI, flaws are first characterized according to established rules and then compared with acceptance criteria.

Flaw Characterization

Flaws detected must be characterized by the flaw length and preferably flaw depth. The proximity rules of Section XI for considering flaws as separate, may be used directly (Section XI, Figure IWA 3400-1). This figure is reproduced here as Figure 6-22.

When a flaw is detected, its projections in both the axial and circumferential directions must be determined. Note that the axial direction is always the same for each penetration, but the circumferential direction will be different depending on the angle of intersection of the penetration nozzle with the vessel head. The "circumferential" direction of interest here is along the top of the attachment weld, as illustrated in Figure 6-23. It is this angle which will change for each penetration nozzle and the top of the attachment weld is also the plane which could cause separation of the penetration nozzle from the vessel head. The location of the flaw relative to both the top and bottom of the partial penetration attachment weld must also be determined since a potential leak path exists when a flaw propagates through the penetration nozzle wall and up the penetration nozzle past the attachment weld. Schematic of a typical weld geometry is shown in Figure 6-24.

Flaw Acceptance Criteria

The maximum allowable depth (a_f) for axial flaws on the inside surface of the penetration nozzle, at or above the weld is 75 percent of the penetration wall thickness. The term a_f is defined as the maximum size to which the detected flaw is calculated to grow in a specified time period. This 75 percent limitation was selected to be consistent with the maximum acceptable flaw depth in Section XI and to provide an additional margin against through wall penetration. There is no concern about separation of the penetration nozzle from the vessel head, unless the flaw is above the attachment weld and oriented circumferentially. Calculations have been completed to show that the geometry of all penetrations can support a continuous circumferential flaw with a depth of 75 percent of the wall thickness.

Axial inside surface flaws found below the weld are acceptable regardless of depth as long as their upper extremity does not reach the bottom of the weld during the period of service until the next inspection. Axial flaws that extend above the weld are limited to 75 percent of the wall thickness.

Axial flaws on the outside surface of the penetration nozzle below the attachment weld are acceptable regardless of depth, as long as they do not extend into the attachment weld during the period of service until next inspection. Outside surface flaws above the attachment weld must be evaluated on a case by case basis, and must be discussed with the regulatory authority.

Circumferential flaws located below the weld are acceptable regardless of their depth, provided the length is less than 75 percent of the penetration nozzle circumference for the period of service until the next inspection. Circumferential flaws detected in this area have no structural

significance except that loose parts must be avoided. To this end, intersecting axial and circumferential flaws shall be removed or repaired. Circumferential flaws at and above the weld must be discussed with the regulatory authority on a case by case basis.

Surface flaws located in the attachment welds themselves are not acceptable regardless of their depth. This is because the crack growth rate is several times faster than that of the Alloy 600 material, and also because depth sizing capability does not yet exist for indications in the attachment weld.

The flaw acceptance criteria are summarized in Table 6-1. Flaws that exceed these criteria must be repaired unless analytically justified for further service. These criteria have been reviewed and approved by the NRC, as documented in references [7, 8] with the exception of the draft criteria discussed above, for outside surface flaws and flaws in the attachment weld. These criteria are identical with the draft acceptance criteria now being considered for Section XI, for head penetrations.

It is expected that the use of these criteria and crack growth curves will provide conservative predictions of the allowable service time.

Table 6-1 Summary of R.V. Head Penetration Flaw Acceptance Criteria (Limits for Future Growth)				
	Axial		Circumferential	
Location	a_f	ℓ	a_f	ℓ
Below Weld (ID)	t	no limit	t	.75 circ.
At and Above Weld (ID)	0.75 t	no limit	*	*
Below Weld (OD)	t	no limit	t	.75 circ.
Above Weld (OD)	*	*	*	*

Note: Surface flaws of any size in the attachment weld are not acceptable.

* Requires case-by-case evaluation and discussion with regulatory authority.

a_f = Flaw Depth
ℓ = Flaw Length
t = Wall Thickness

Table 6-2 St. Lucie Unit 2 Penetration Geometries [11A, 11B, 11C]		
Penetration Type	Wall Thickness (in.)	Penetration OD (in.)
CEDM	0.661	4.050
ICI	0.469*	5.563
ICI Counterbore	0.407*	5.563
Head Vent	0.154	1.050

* ICI Counterbore wall thickness shall be used when evaluating ICI nozzle flaws at all time.

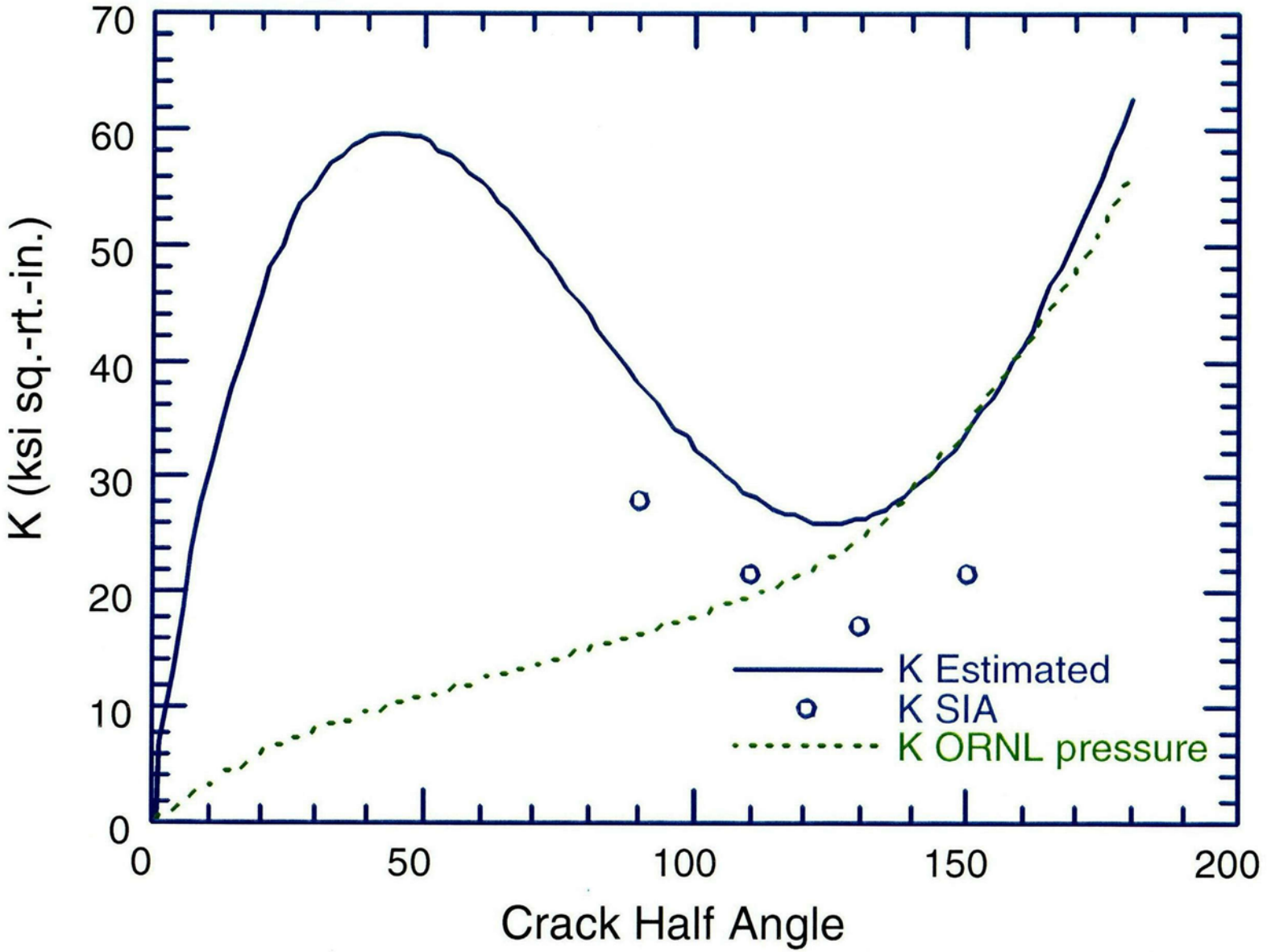

Figure 6-1 Stress Intensity Factor for a Through-Wall Circumferential Flaw in a Head Penetration

C10

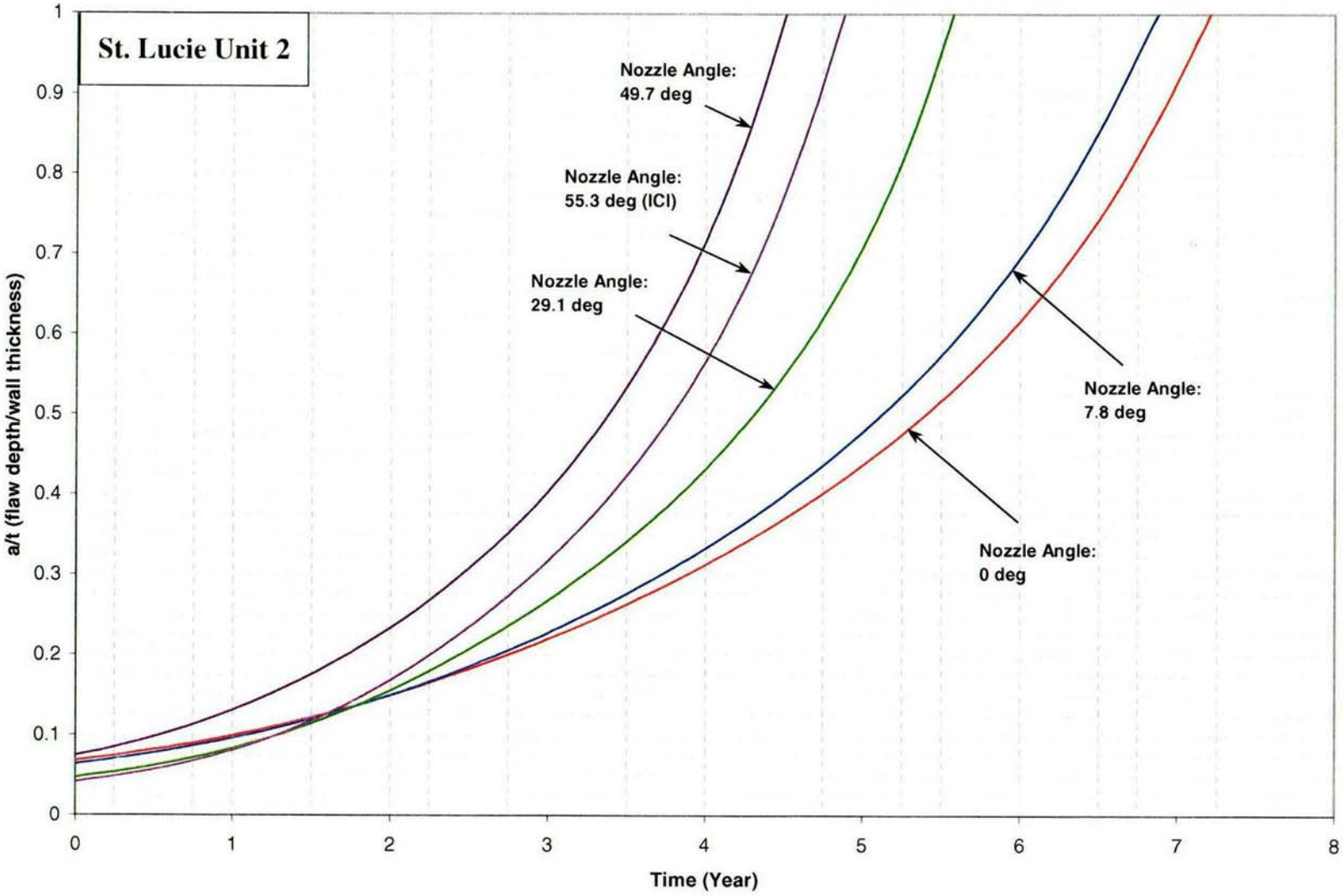

Figure 6-2 Inside, Axial Surface Flaws, .5" Below the Attachment Weld, Nozzle Uphill Side - Crack Growth Predictions

C11

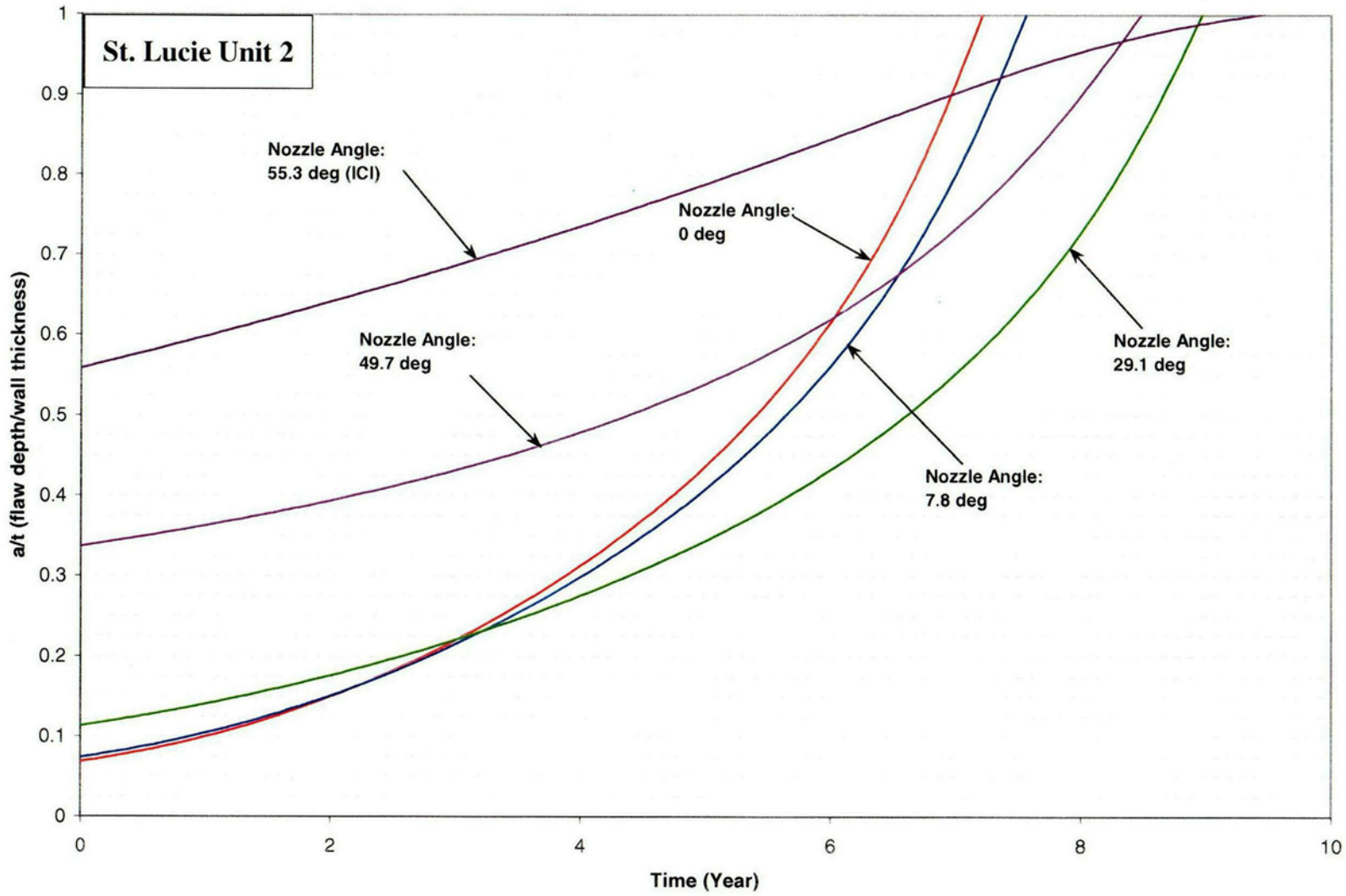

Figure 6-3 Inside, Axial Surface Flaws, .5" Below the Attachment Weld, Nozzle Downhill Side - Crack Growth Predictions

C12

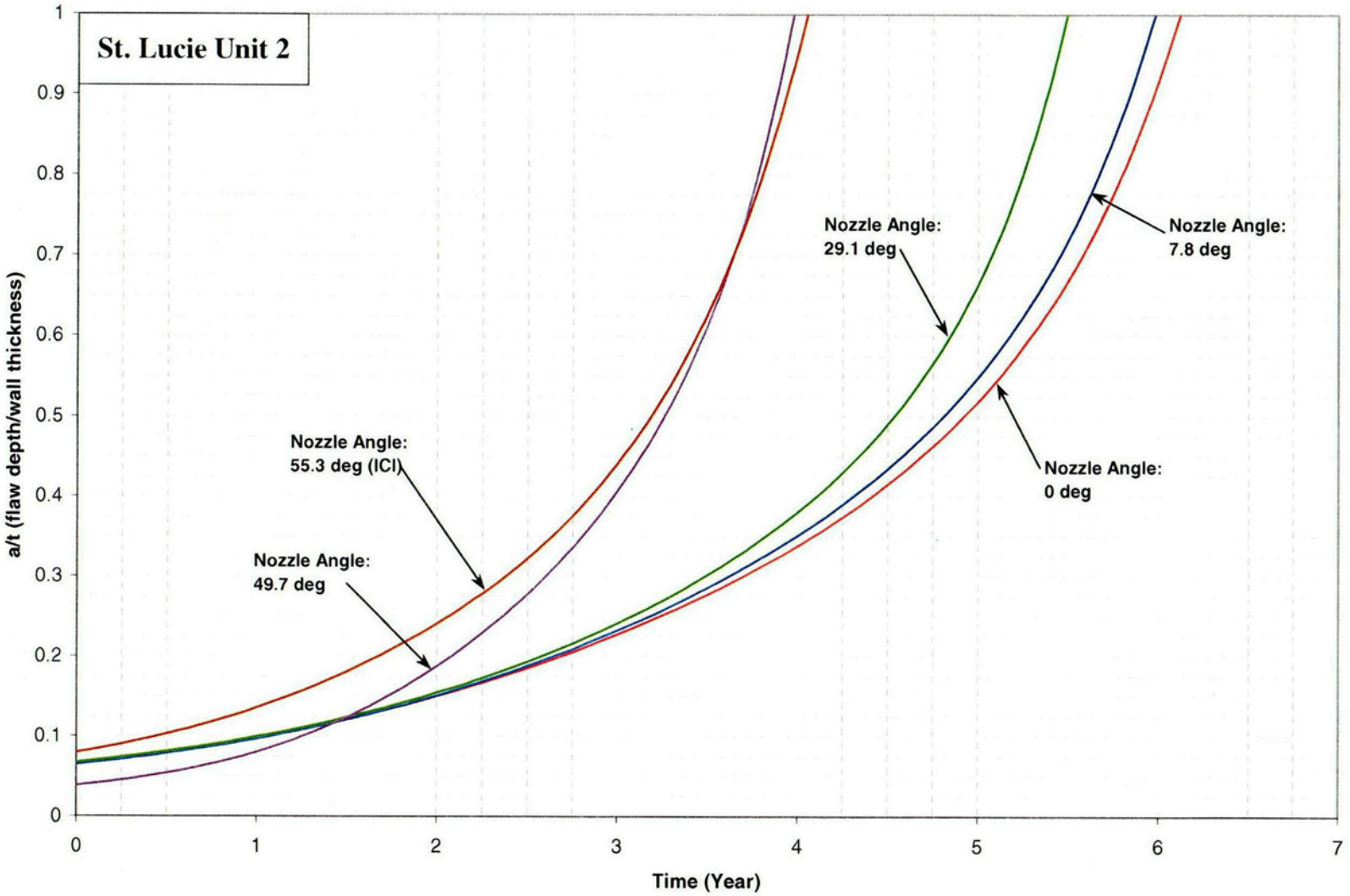

Figure 6-4 Inside, Axial Surface Flaws, At the Attachment Weld, Nozzle Uphill Side - Crack Growth Predictions

C13

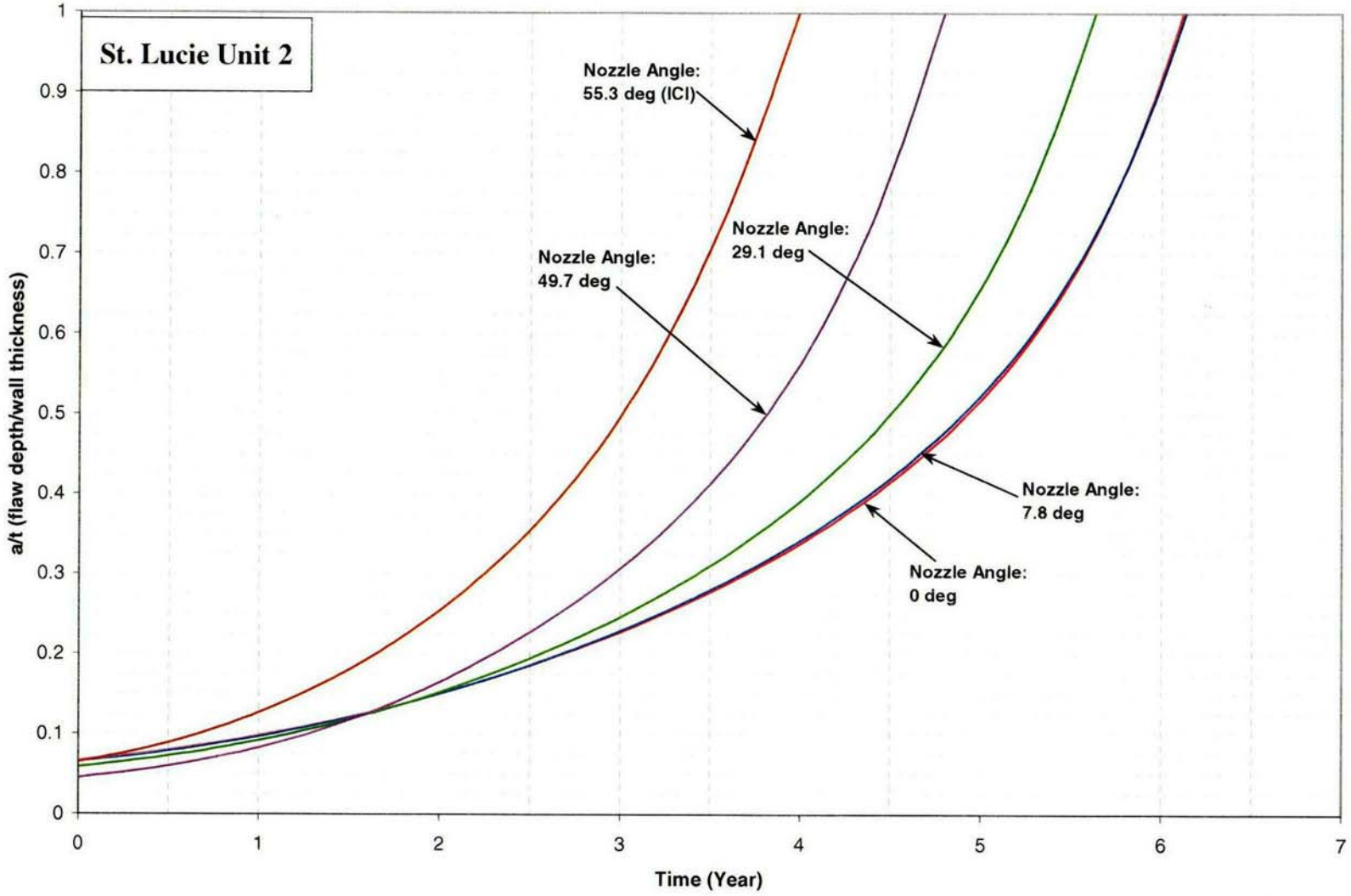

Figure 6-5 Inside, Axial Surface Flaws, At the Attachment Weld, Nozzle Downhill Side - Crack Growth Predictions

C14

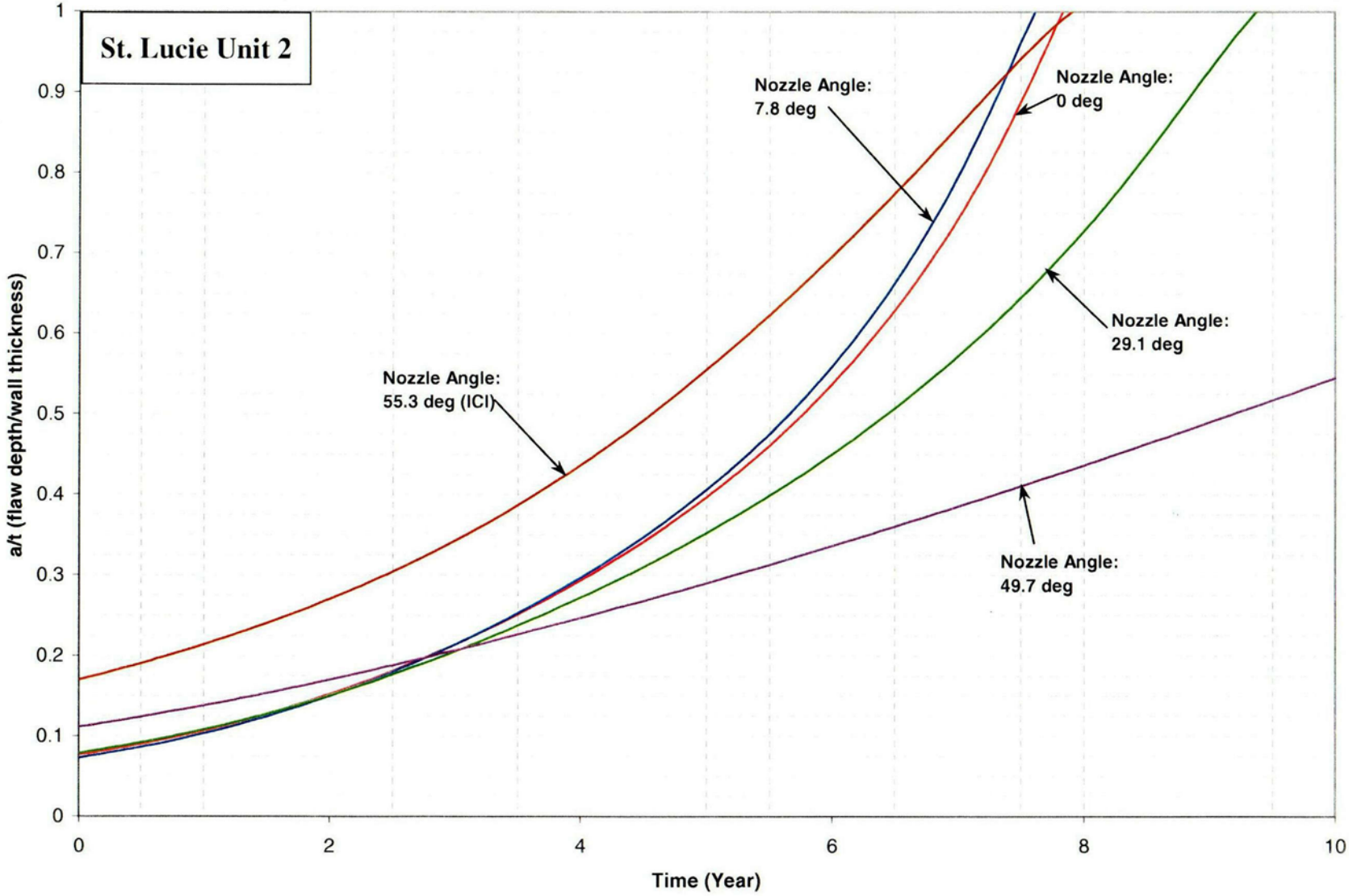

Figure 6-6 Inside, Axial Surface Flaws, .5" Above the Attachment Weld, Nozzle Uphill Side - Crack Growth Predictions

C15

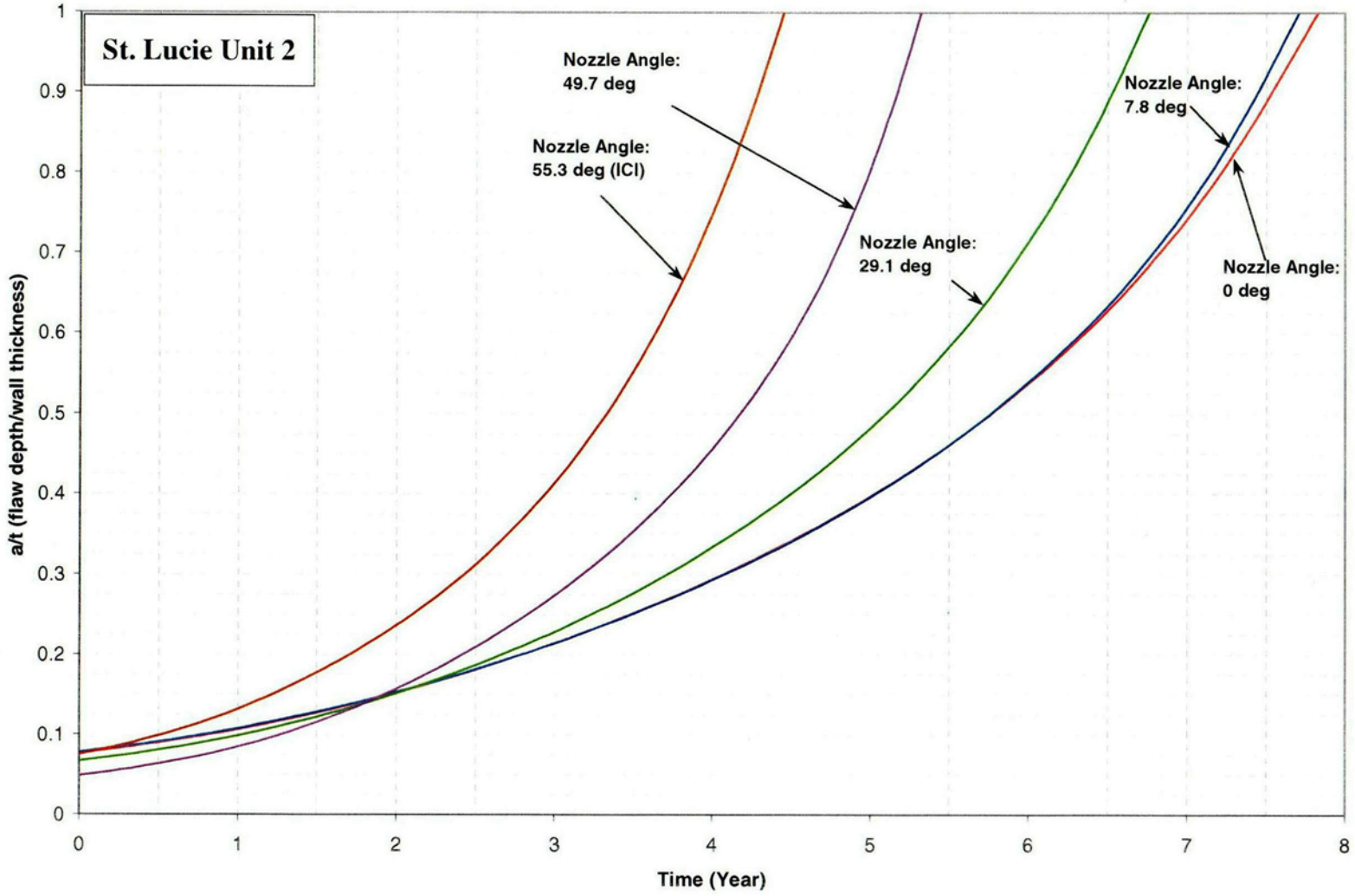

Figure 6-7 Inside, Axial Surface Flaws, .5" Above the Attachment Weld, Nozzle Downhill Side - Crack Growth Predictions

C16

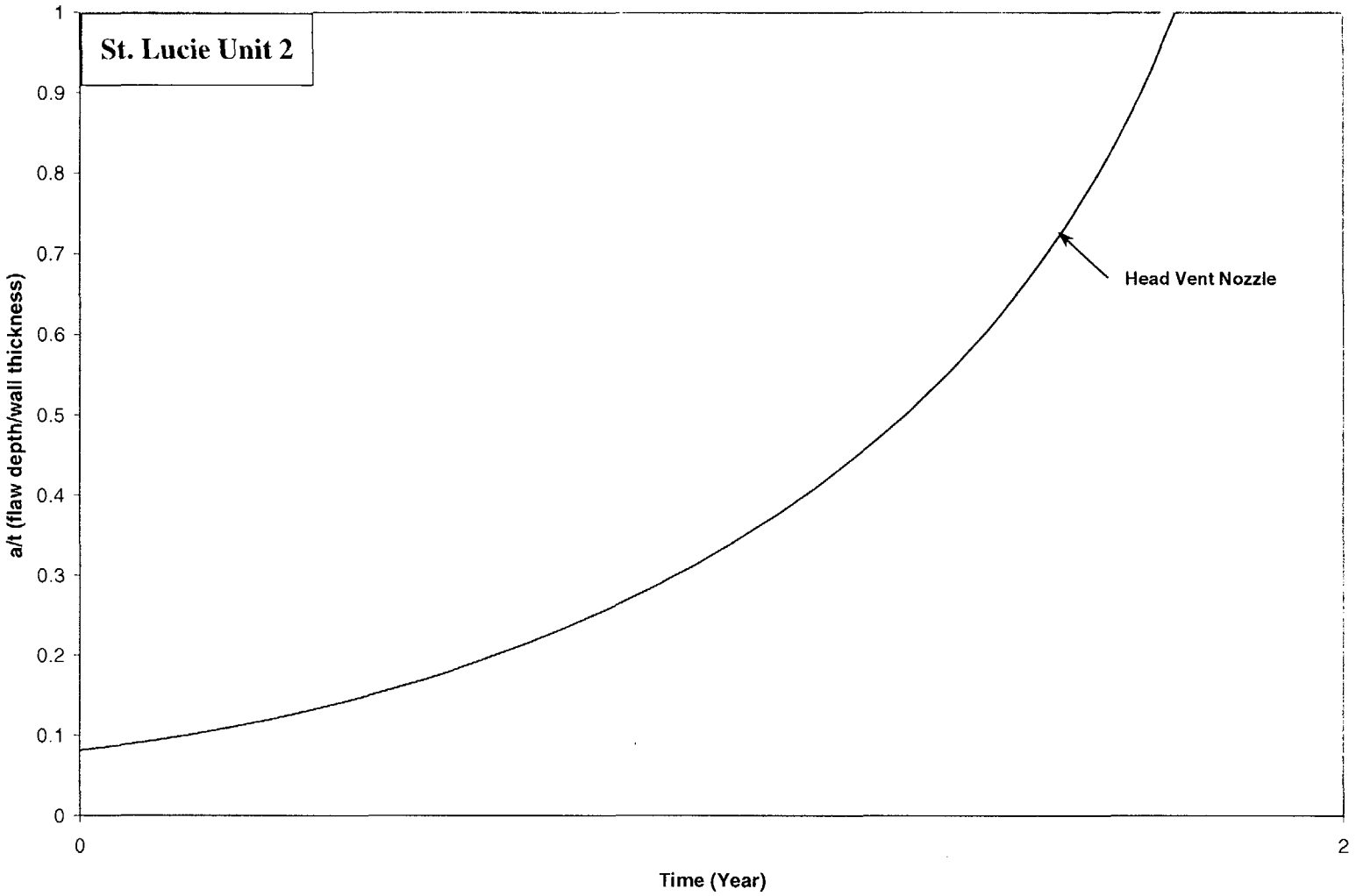

Figure 6-8 Inside, Axial Surface Flaws, At the Attachment Weld, Head Vent, Nozzle Downhill Side - Crack Growth Predictions

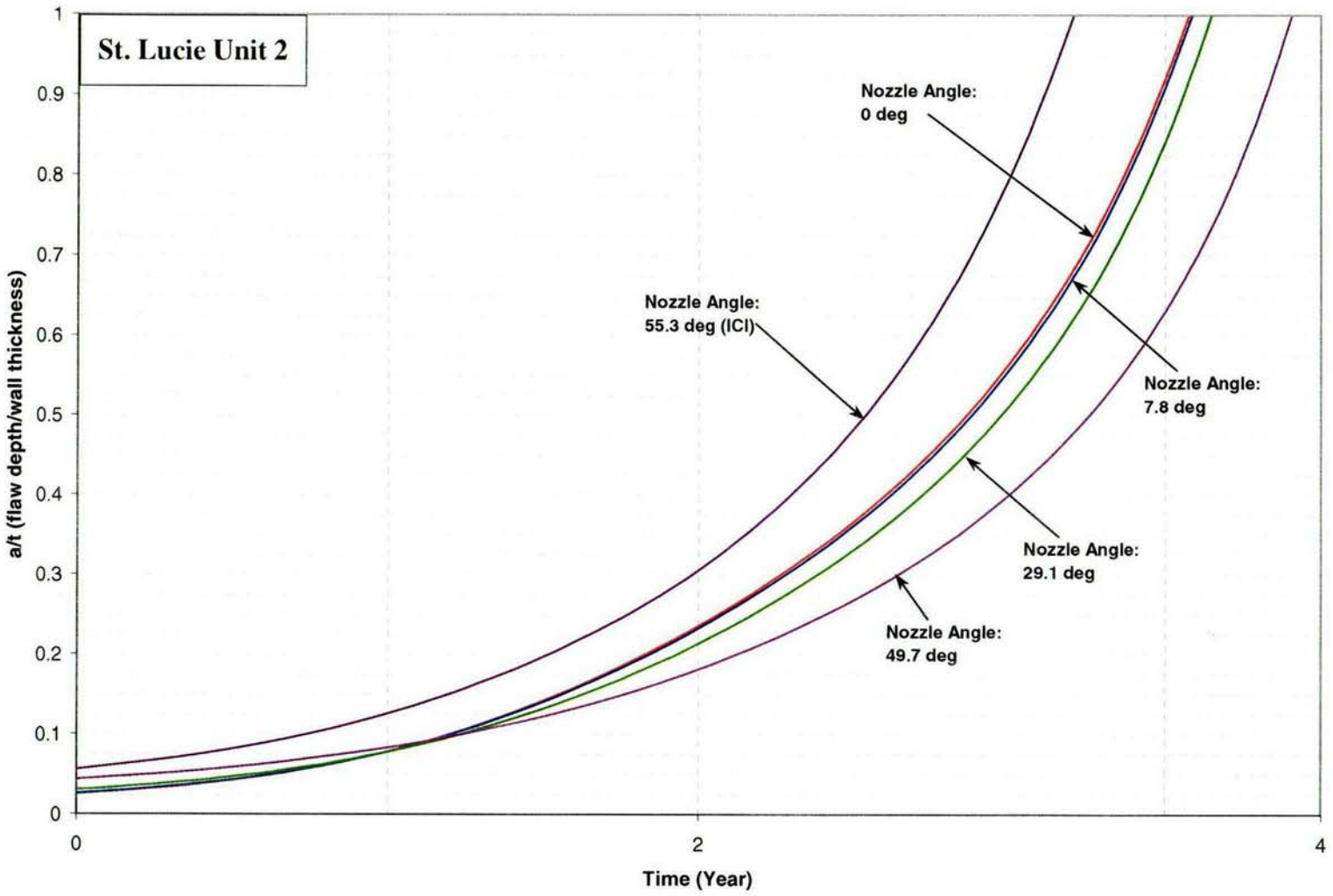

Figure 6-9 Outside, Axial Surface Flaws, Below the Attachment Weld, Nozzle Uphill Side - Crack Growth Predictions

C17

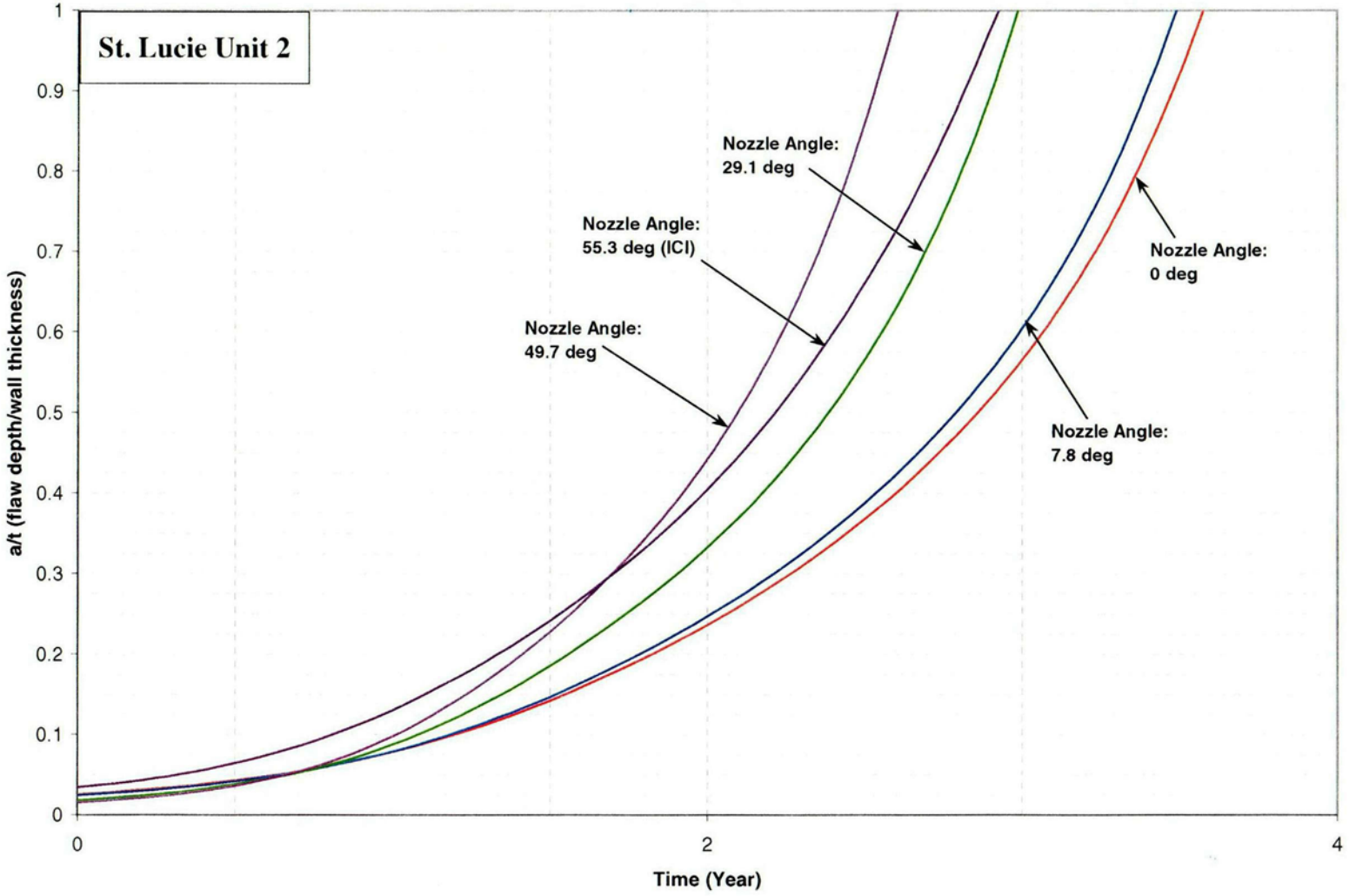

Figure 6-10 Outside, Axial Surface Flaws, Below the Attachment Weld, Nozzle Downhill Side - Crack Growth Predictions

C10

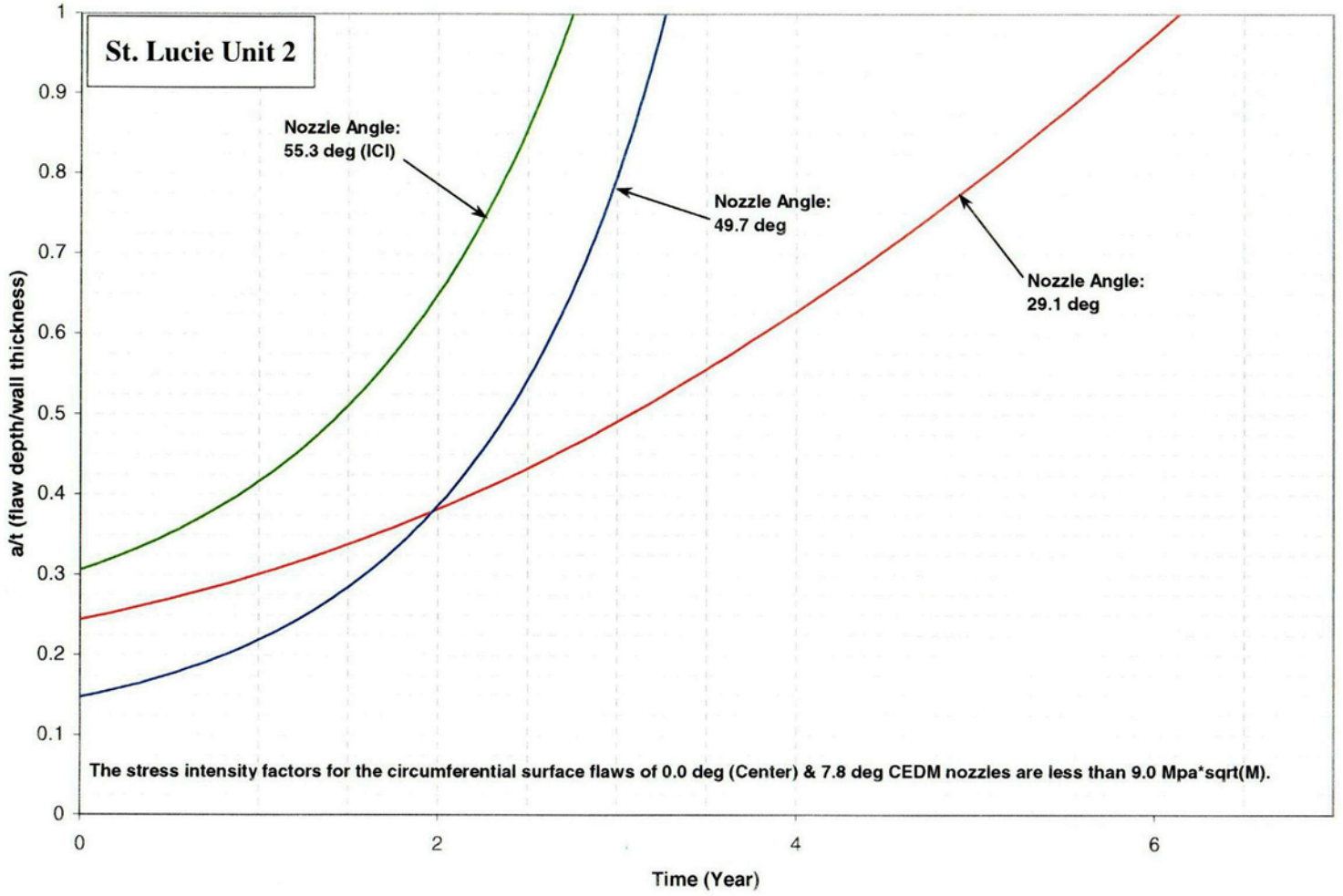

Figure 6-11 Outside, Circumferential Surface Flaws, Along the Top of the Attachment Weld - Crack Growth Predictions (MRP Factor of 2.0 Included)

C19

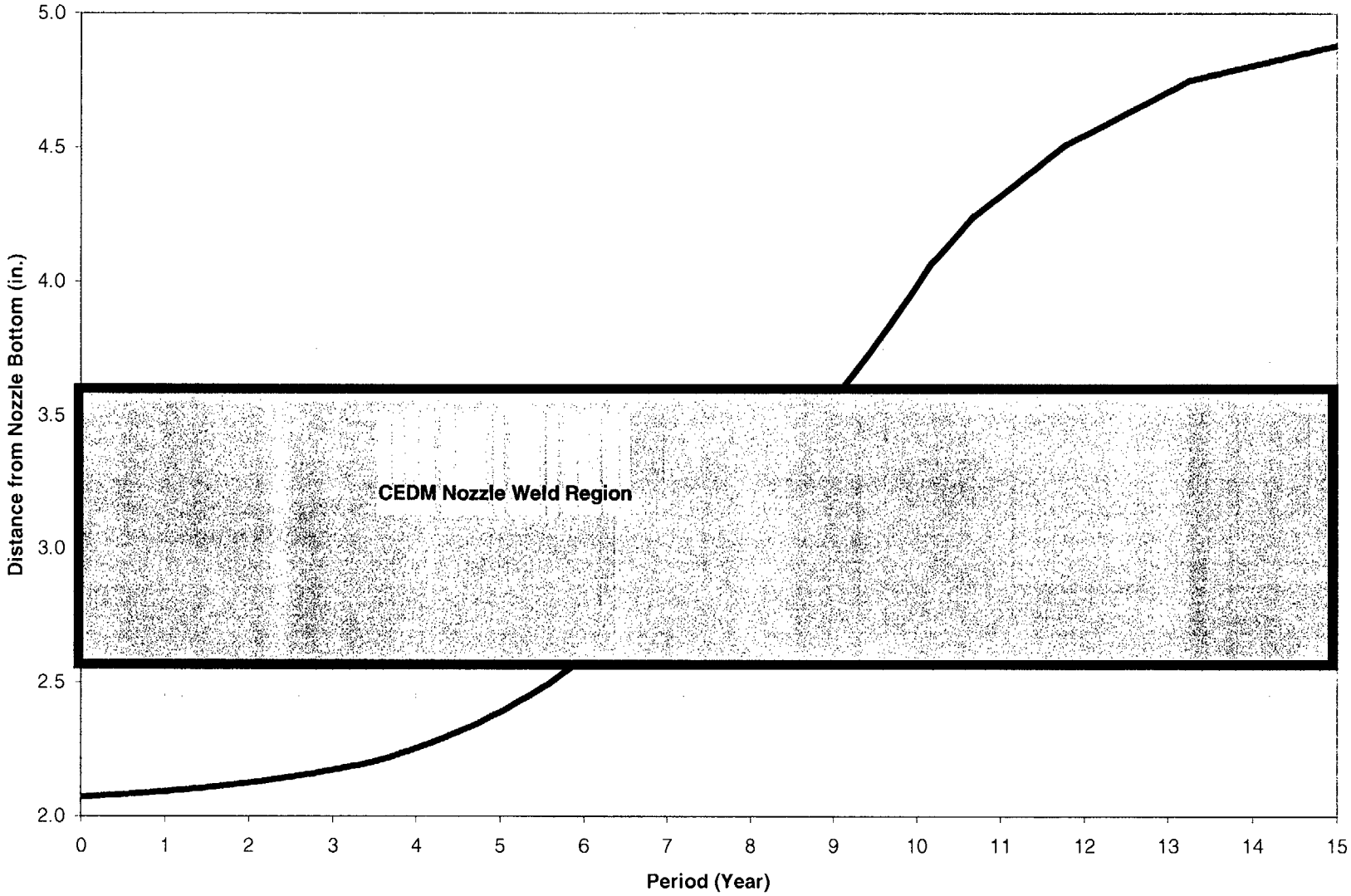

Figure 6-12 Through-Wall Axial Flaws Located in the Center CEDM (0.0 Degrees) Penetration, Uphill and Downhill Side - Crack Growth Predictions

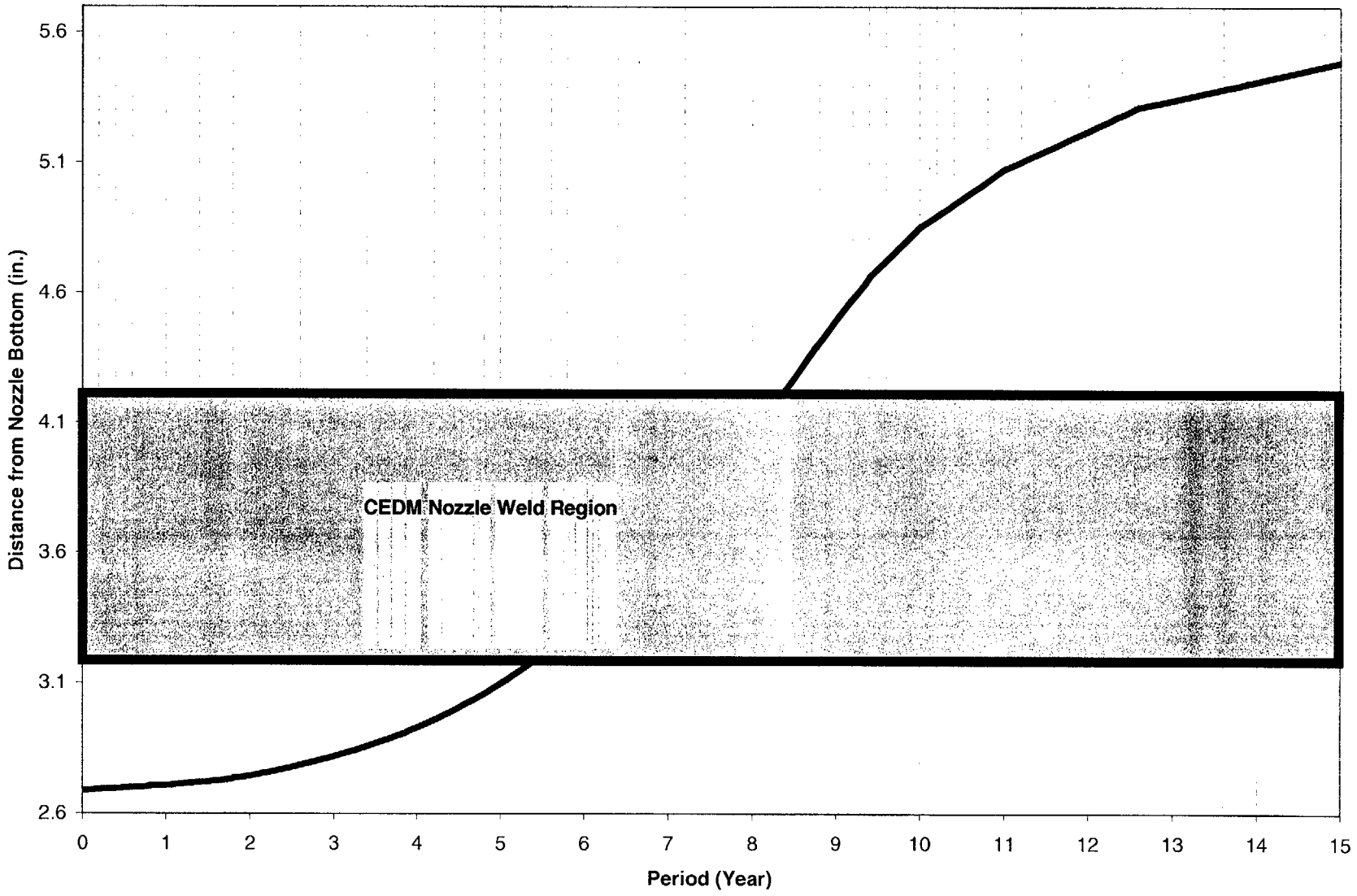

Figure 6-13 Through-Wall Axial Flaws Located in the 7.8 Degrees Row of Penetrations, Uphill Side - Crack Growth Predictions

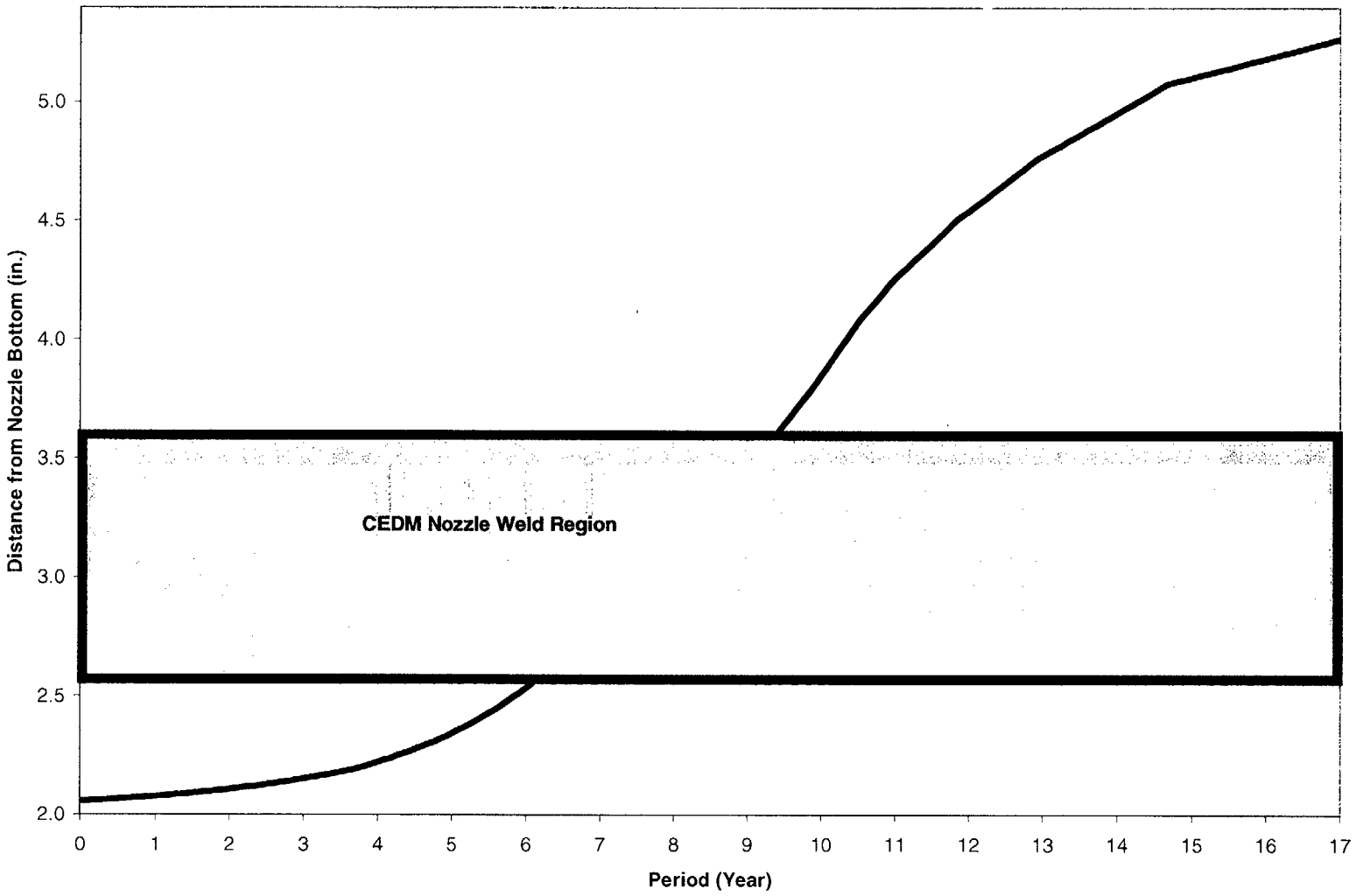

Figure 6-14 Through-Wall Axial Flaws Located in the 7.8 Degrees Row of Penetrations, Downhill Side - Crack Growth Predictions

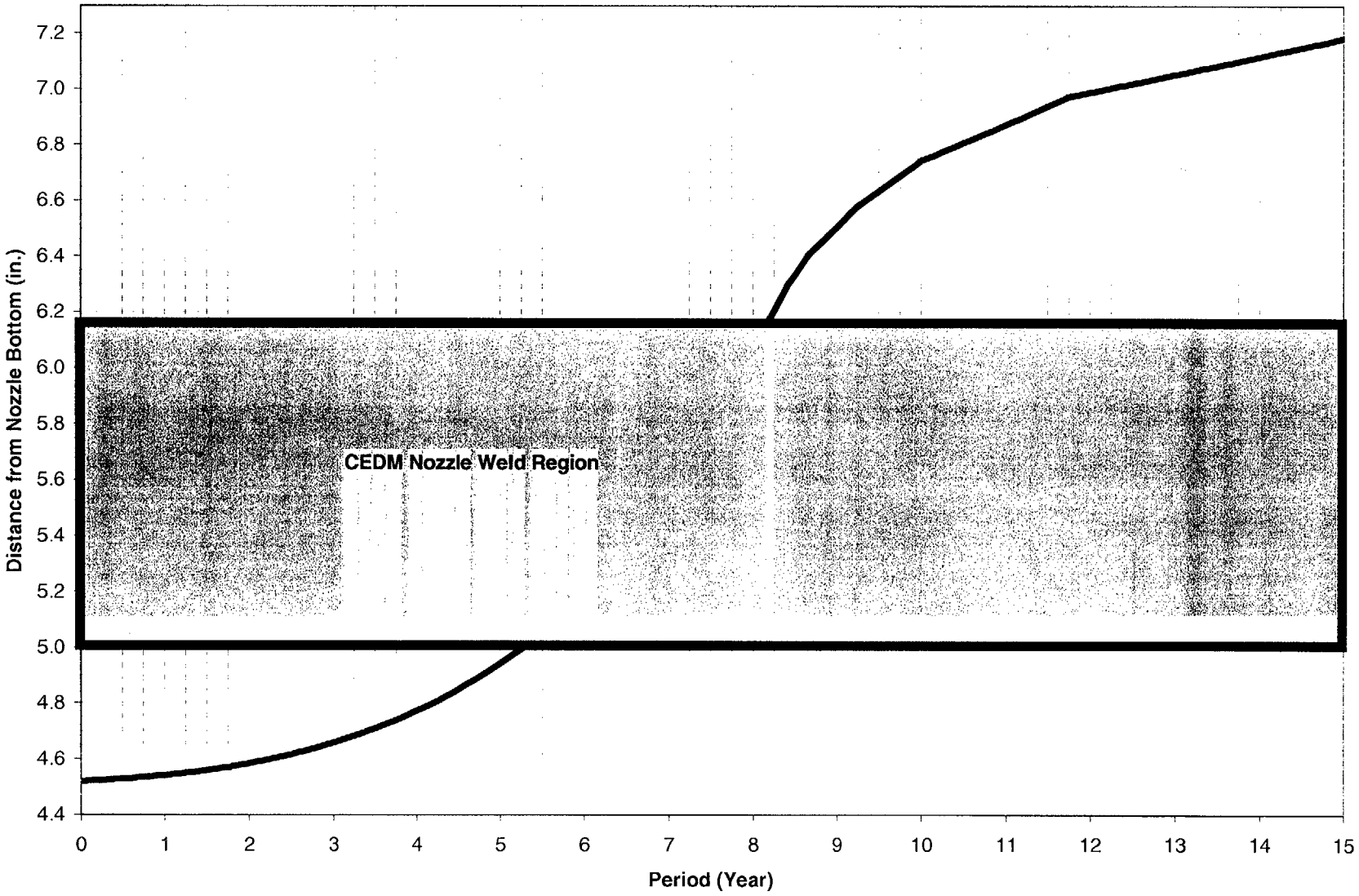

Figure 6-15 Through-Wall Axial Flaws Located in the 29.1 Degrees Row of Penetrations, Uphill Side - Crack Growth Predictions

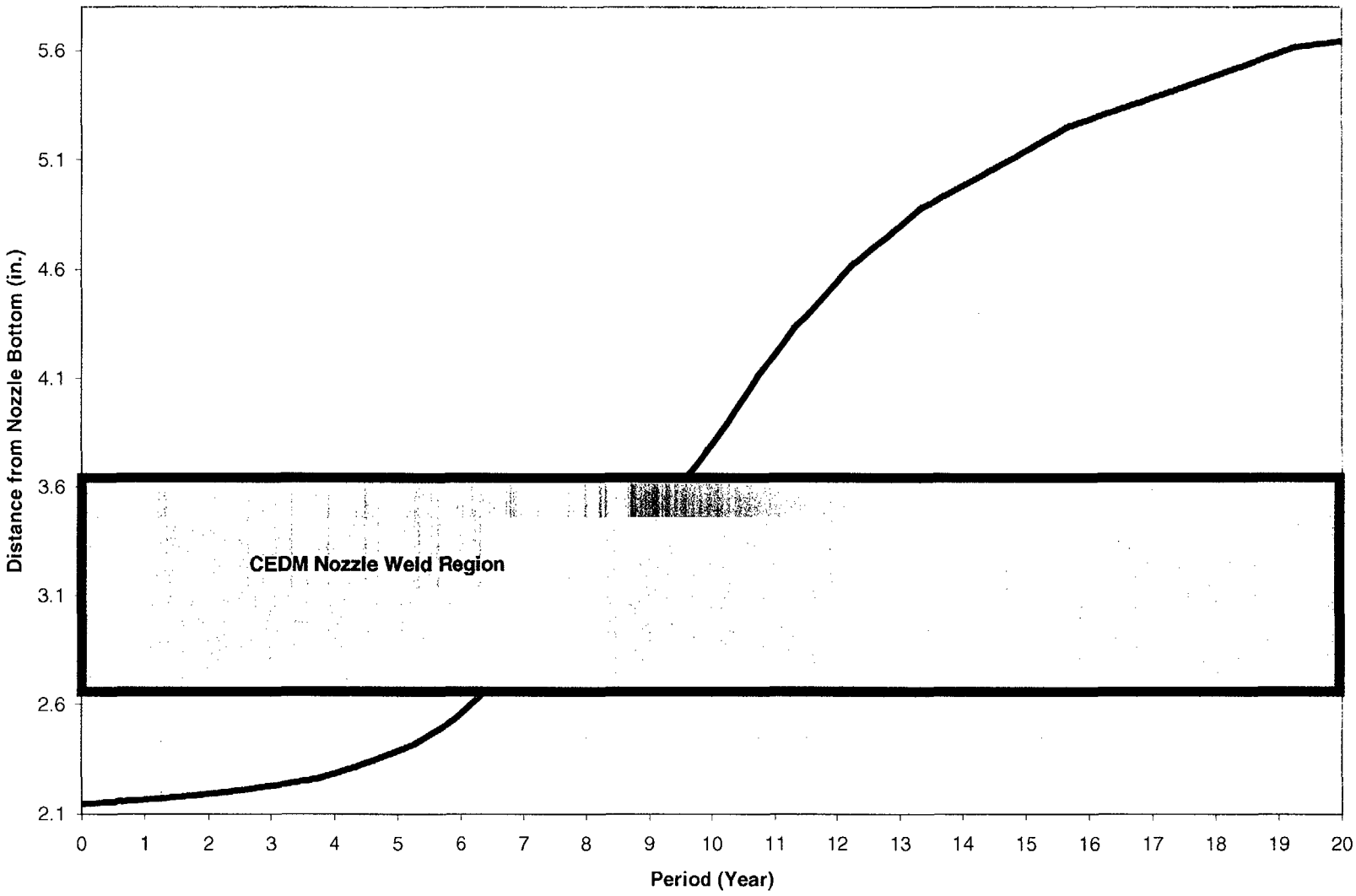

Figure 6-16 Through-Wall Axial Flaws Located in the 29.1 Degrees Row of Penetrations, Downhill Side - Crack Growth Predictions

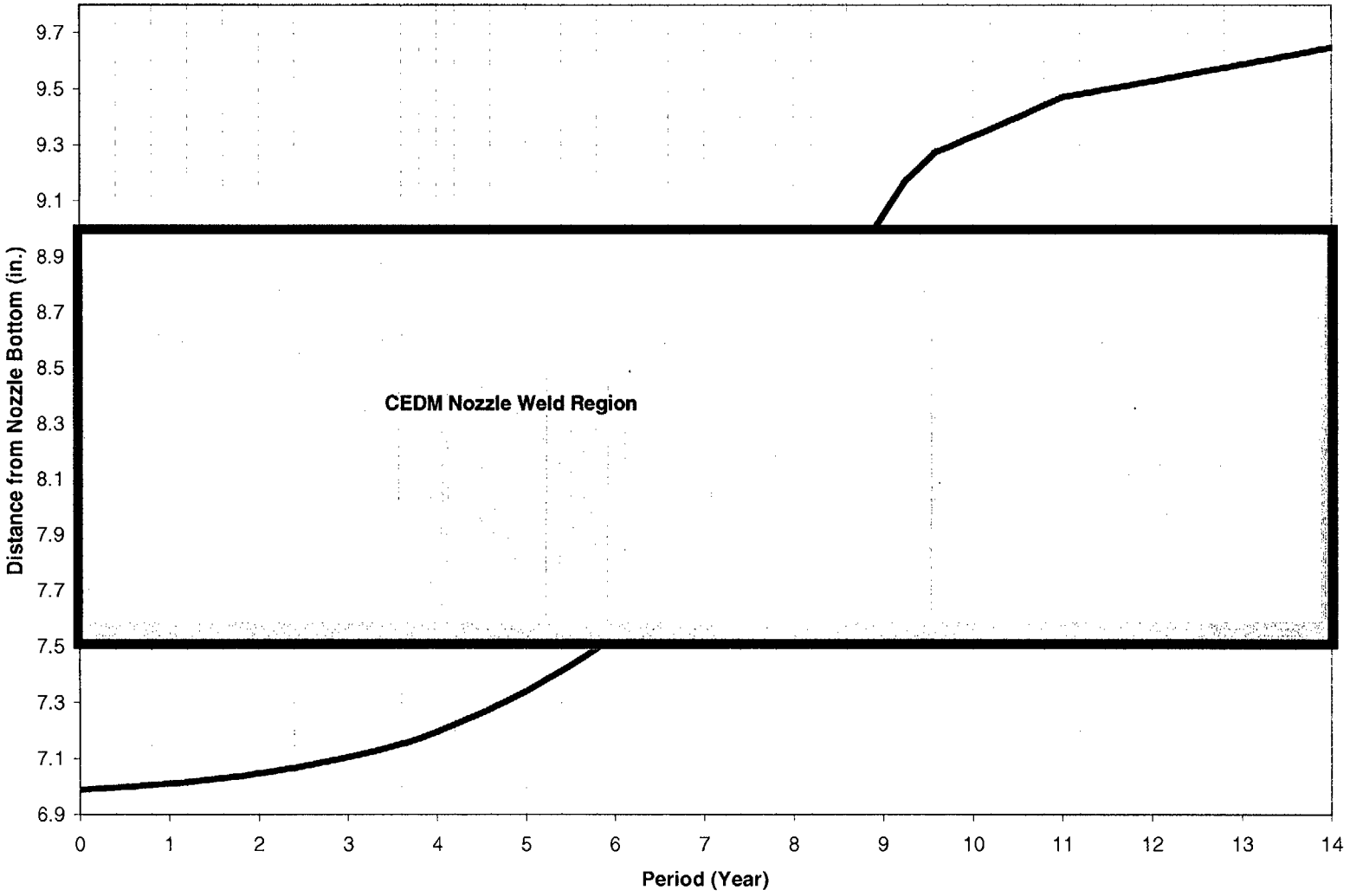

Figure 6-17 Through-Wall Axial Flaws Located in the 49.7 Degrees Row of Penetrations, Uphill Side - Crack Growth Predictions

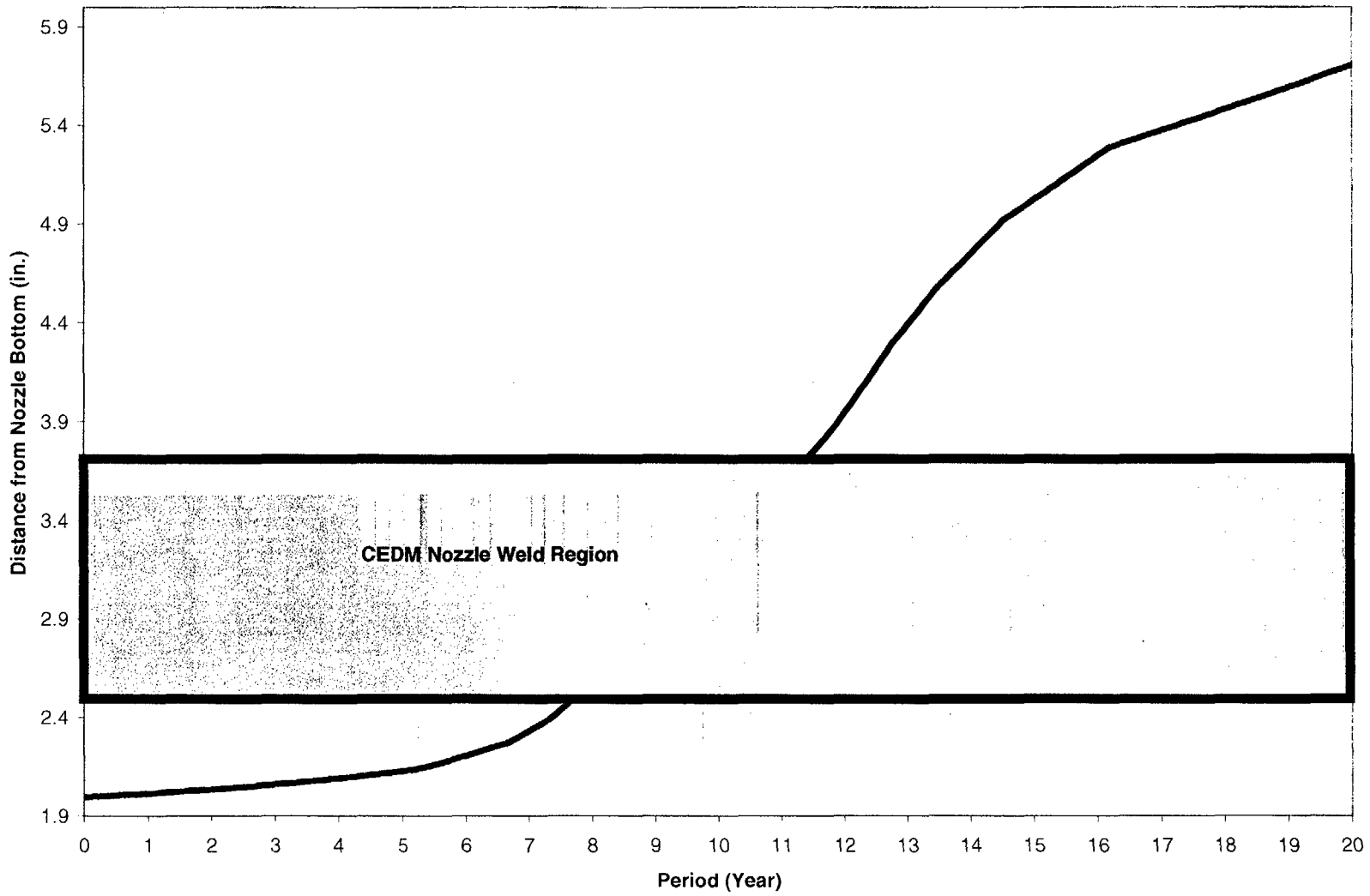

Figure 6-18 Through-Wall Axial Flaws Located in the 49.7 Degrees Row of Penetrations, Downhill Side - Crack Growth Predictions

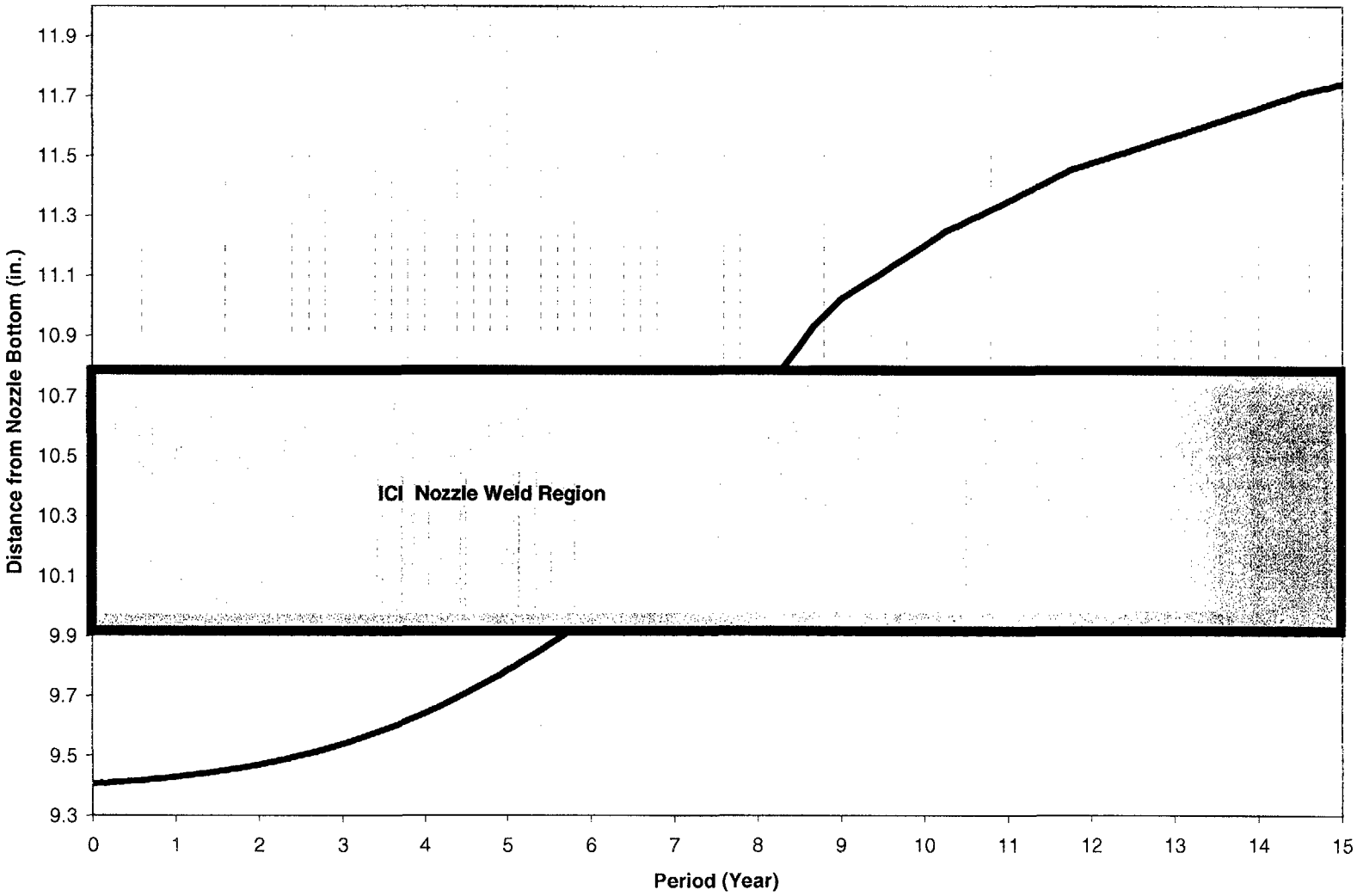

Figure 6-19 Through-Wall Axial Flaws Located in the 55.3 Degrees Row of Penetrations, Uphill Side - Crack Growth Predictions

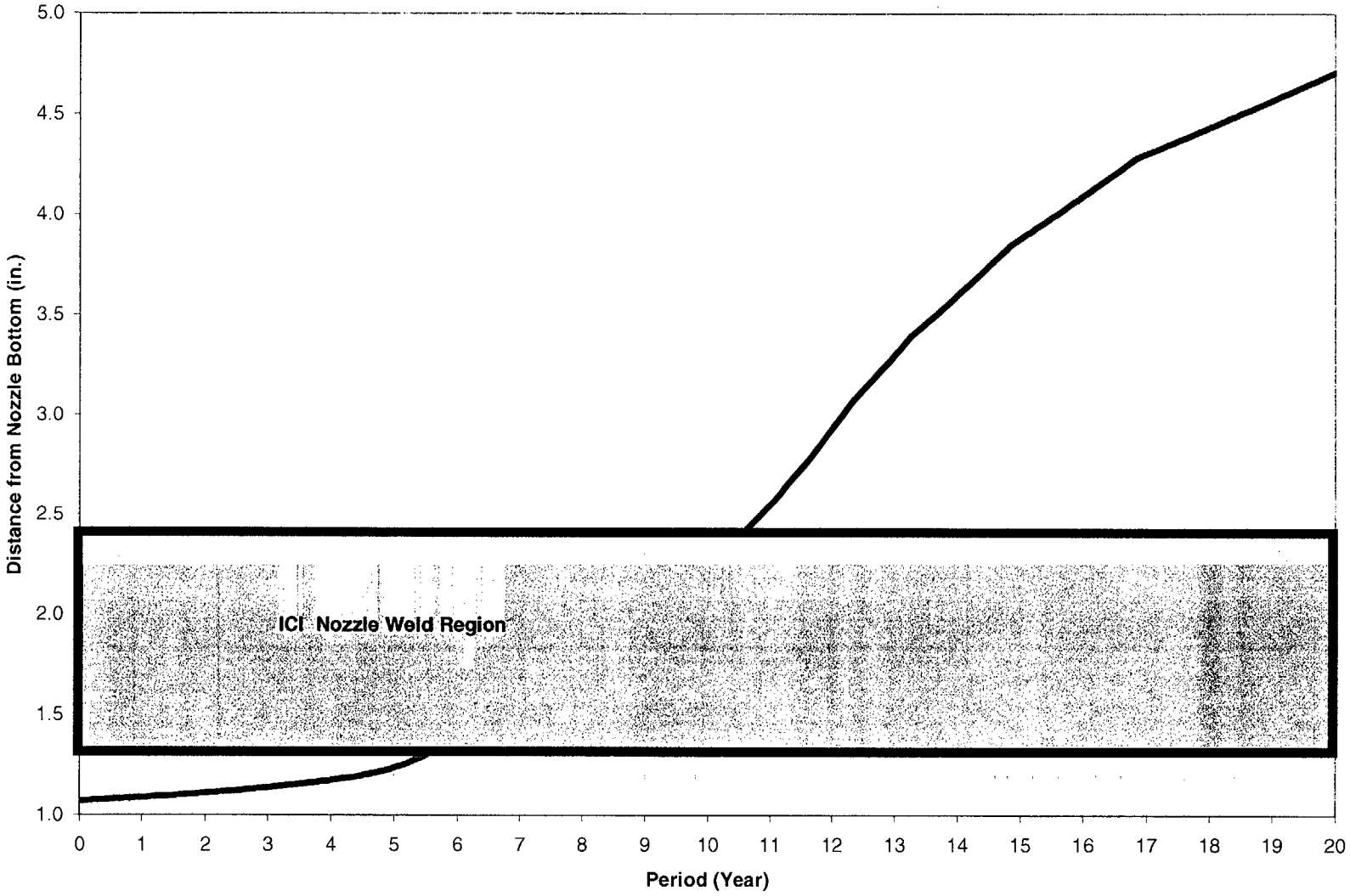

Figure 6-20 Through-Wall Axial Flaws Located in the 55.3 Degrees Row of Penetrations, Downhill Side - Crack Growth Predictions

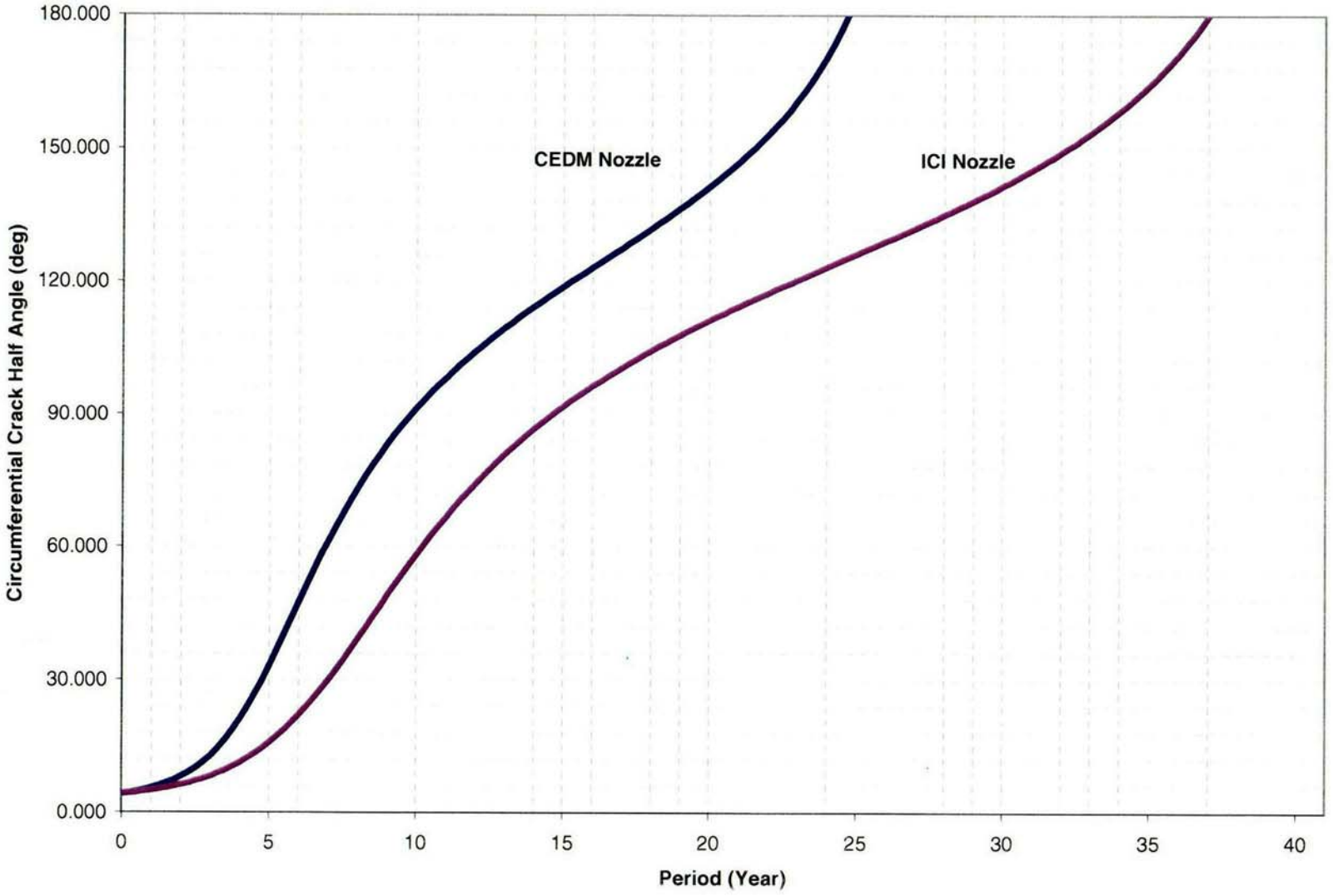

Figure 6-21 Through-Wall Circumferential Flaws Near the Top of the Attachment Weld for CEDM and ICI Nozzles - Crack Growth Predictions (MRP Factor of 2.0 Included)

C20

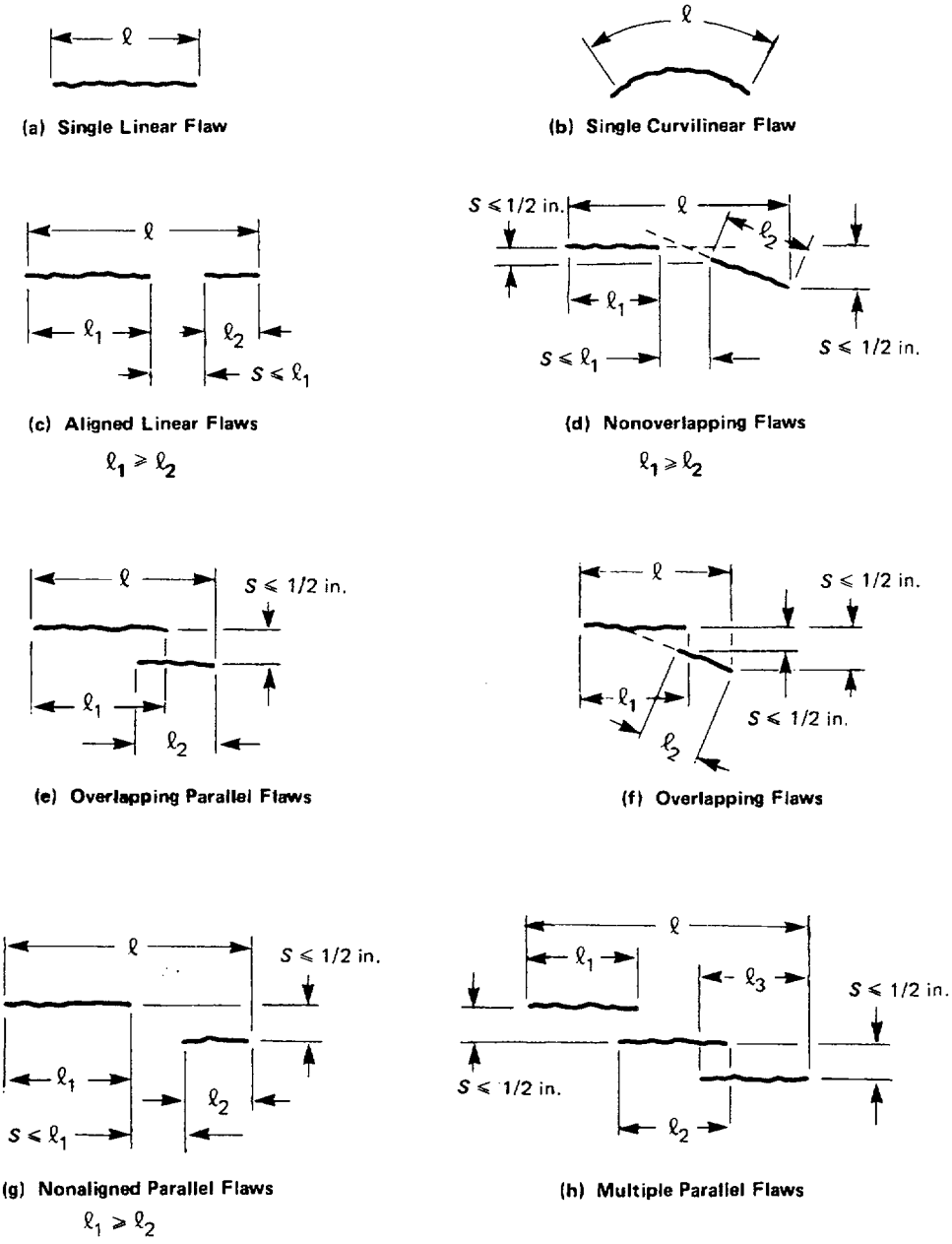

Figure 6-22 Section XI Flaw Proximity Rules for Surface Flaws (Figure IWA-3400-1)

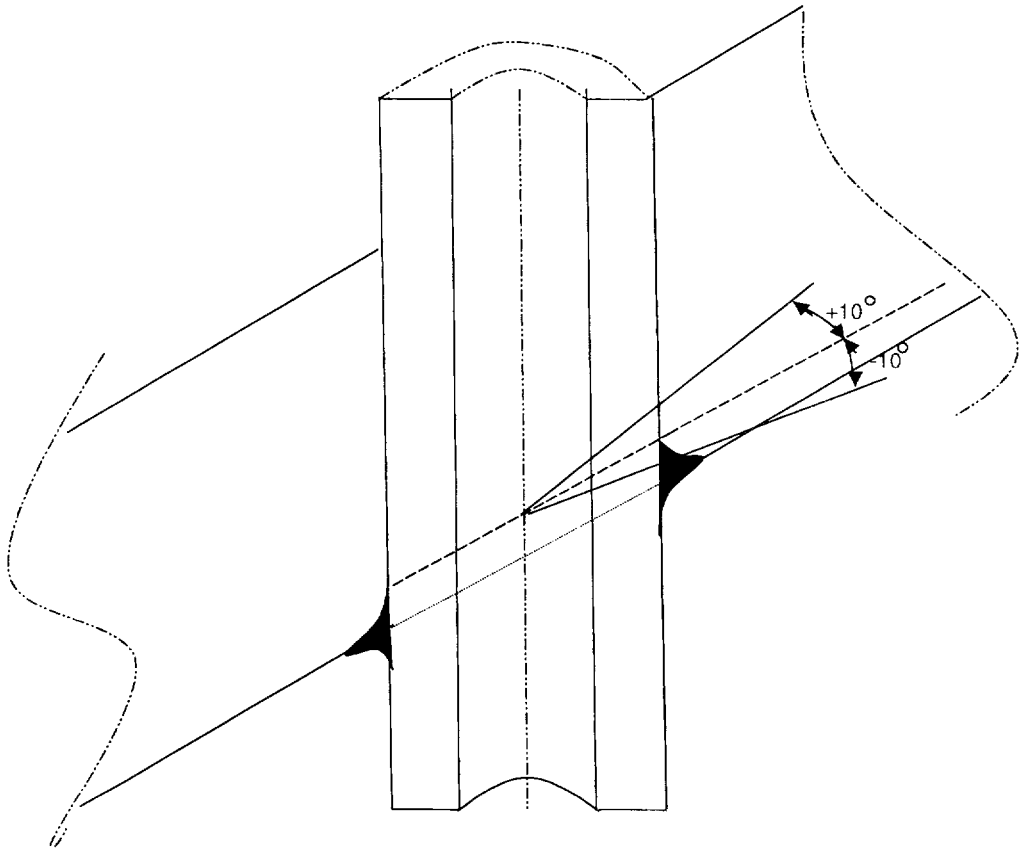

Figure 6-23 Definition of "Circumferential"

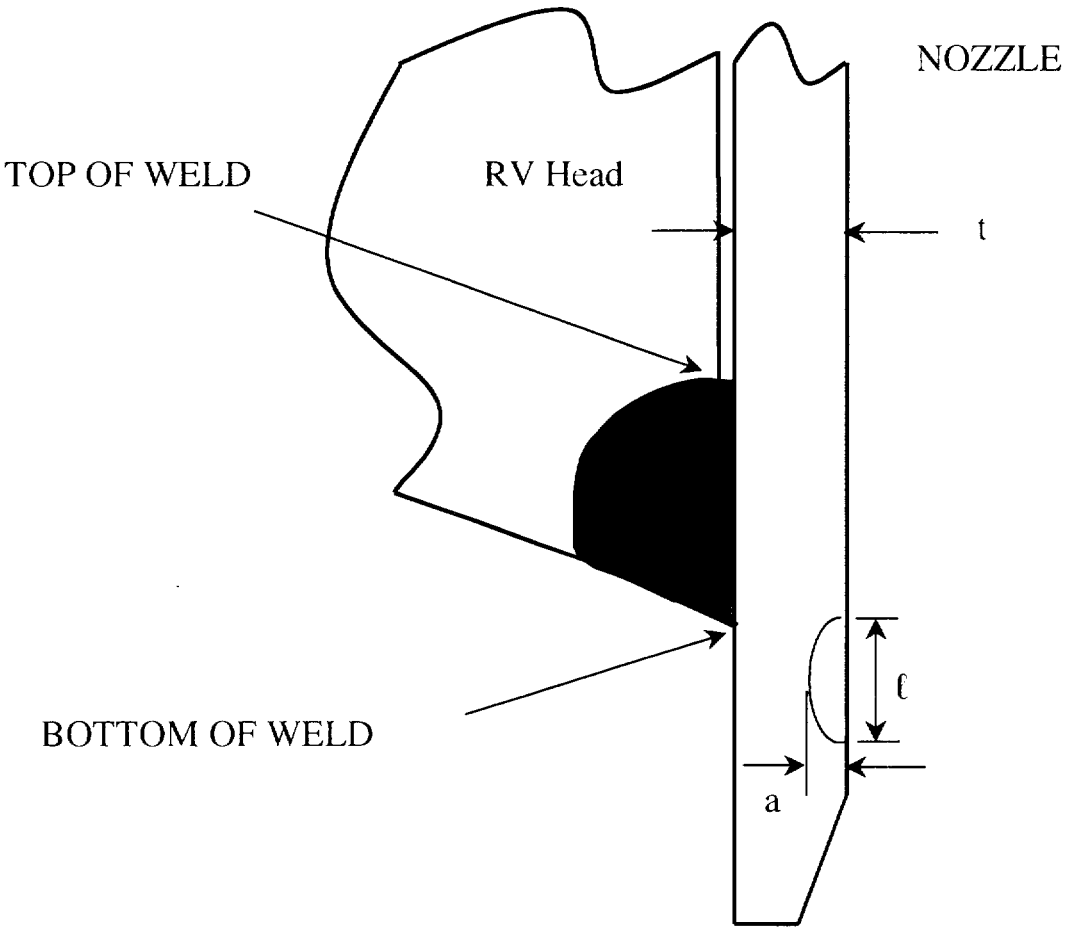

Figure 6-24 Schematic of Head Penetration Geometry